ISSN 8755-6839

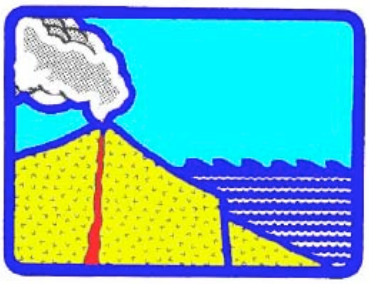

SCIENCE OF TSUNAMI HAZARDS

The International Journal of The Tsunami Society
Volume 28 Number 5 Published Electronically 2009

TSUNAMI SOCIETY INTERNATIONAL, 1741 Ala Moana Blvd. #70, Honolulu, HI 96815,USA.

WWW.TSUNAMISOCIETY.ORG

SCIENCE OF TSUNAMI HAZARDS is a CERTIFIED OPEN ACCESS Journal included in the prestigious international academic journal database DOAJ maintained by the University of Lund in Sweden with the support of the European Union. 'SCIENCE OF TSUNAMI HAZARDS is also preserved and archived at the National Library, The Hague, NETHERLANDS, at the Library of Congress, Washington D.C., USA, and in the Electronic Library of Los Alamos, National Laboratory, New Mexico, USA.

OBJECTIVE: The Tsunami Society publishes this journal to increase and disseminate knowledge about tsunamis and their hazards.

DISCLAIMER: Although these articles have been technically reviewed by peers, the Tsunami Society is not responsible for the veracity of any statement, opinion or consequences.

Submit manuscripts of articles, notes or letters to the Editor. If an article is accepted for publication the author(s) must submit a scan ready manuscript, a Doc, TeX or a PDF file in the journal format. Issues of the journal are published electronically in PDF format. Recent journal issues are available at: http://www.TsunamiSociety.org http://www.sthjournal.org

Tsunami Society members will be advised by e-mail when a new issue is available. There are no page charges for one paper per calendar year for authors who are members of Tsunami Society International. Permission to use figures, tables and brief excerpts from this journal in scientific and educational works is hereby granted provided that the source is acknowledged.

Issues of the journal (ISSN 8755-6839) from 1982 thru 2005 are available in PDF format at http://epubs.lanl.gov/tsunami/ and at **WWW.TSUNAMISOCIETY.ORG** or on a CD-ROM that may be purchased by contacting Tsunami Society International at tsunamisociety@hawaiiantel.net

COMPARING SEA LEVEL RESPONSE AT MONTEREY, CALIFORNIA FROM THE 1989 LOMA PRIETA EARTHQUAKE AND THE 1964 GREAT ALASKAN EARTHQUAKE

L. C. Breaker[1], T.S. Murty[2], Jerrold G. Norton[3], & Dustin Carroll[1]

[1]Moss Landing Marine Laboratories, Moss Landing, California
[2] University of Ottawa, Ottawa, Canada
[3] Southwest Fisheries Science Center/NMFS/NOAA, La Jolla, California
Email: mailto:Lbreaker@mlml.calstate.edu

ABSTRACT

Two of the largest earthquakes to affect water levels in Monterey Bay in recent years were the Loma Prieta Earthquake (LPE) of 1989 with a moment magnitude of 6.9, and the Great Alaskan Earthquake (GAE) of 1964 with a moment magnitude of 9.2. In this study, we compare the sea level response of these events with a primary focus on their frequency content and how the bay affected it, itself. Singular Spectrum Analysis (SSA) was employed to extract the primary frequencies associated with each event. It is not clear how or exactly where the tsunami associated with the LPE was generated, but it occurred inside the bay and most likely began to take on the characteristics of a seiche by the time it reached the tide gauge in Monterey Harbor. Results of the SSA decomposition revealed two primary periods of oscillation, 9-10 minutes, and 31-32 minutes. The first oscillation is in agreement with the range of periods for the expected natural oscillations of Monterey Harbor, and the second oscillation is consistent with a bay-wide oscillation or seiche mode. SSA decomposition of the GAE revealed several sequences of oscillations all with a period of approximately 37 minutes, which corresponds to the predicted, and previously observed, transverse mode of oscillation for Monterey Bay. In this case, it appears that this tsunami produced quarter-wave resonance within the bay consistent with its seiche-like response. Overall, the sea level responses to the LPE and GAE differed greatly, not only because of the large difference in their magnitudes but also because the driving force in one case occurred inside the bay (LPE), and in the second, outside the bay (GAE). As a result, different modes of oscillation were excited.

Science of Tsunami Hazards, Vol. 28, No. 5, page 255 (2009)

1. INTRODUCTION

In the past 50 years, two of the largest earthquakes to affect water levels in Monterey Bay were the Loma Prieta Earthquake of 1989 and the Great Alaskan Earthquake of 1964. The epicenter of the Loma Prieta Earthquake (LPE) occurred relatively close to Monterey Bay (Fig. 1) and the bay was part of the area affected by the event whereas the Great Alaskan Earthquake (GAE) occurred in Prince William Sound, Alaska, over 3000 km northwest of Monterey Bay. Also, the magnitude of these events differed greatly. Whereas the LPE had a surface-wave magnitude of 7.1, the GAE had a surface-wave magnitude of 8.3 on the Richter scale. Additionally, the tsunami associated with the LPE was generated inside the bay whereas the tsunami associated with the GAE was generated near the epicenter in the northern Gulf of Alaska, propagated as a tsunami across the Pacific basin and down the west coast of North America and was then transformed into a seiche upon entering Monterey Bay. In each case, these events were recorded at a tide gauge at 36°36.3', 121°53.3' in Monterey Harbor located in the inner bight of southern Monterey Bay. Fig. 1 shows Monterey Bay, the epicenter for the LPE, and certain aspects of the tsunamis and seiches associated with each event.

Figure 1. This figure shows Monterey Bay and depictions of the 1964 Great Alaskan Earthquake (GAE) tsunami (outside the bay) and the corresponding seiche (inside the bay), and the 1989 Loma Prieta Earthquake (LPE) tsunami and seiche (both inside the bay). The dotted line across the entrance of the bay represents the assumed location of the nodal line that corresponds to the node for transverse oscillations whose orientation is orthogonal to this line.

The natural oscillations of Monterey Bay, or seiche modes, have been a topic of interest for at least 40 years. Wilson, Hendrickson, and Kilmer (1965) examined the oscillating characteristics of Monterey Bay using a number of analytical and numerical techniques to estimate the expected periods of oscillation. Analytical and numerical methods were applied using various simple geometrical shapes to approximate the bay in order to extract its natural modes of oscillation. In applying these methods, a nodal line was assumed to exist across the mouth of the bay from the Monterey Peninsula to Santa Cruz (Fig. 1). In describing the oscillating characteristics of the bay, the mode of oscillation oriented in the North-South direction that spans the bay is referred to as longitudinal, and the mode of oscillation oriented in the East-West direction, where the existence of a nodal line is assumed, is referred to as transverse. The results of Wilson, Hendrickson, and Kilmer (1965) indicated that in addition to longitudinal and transverse modes of oscillation, many higher modes of oscillation can be excited that are primarily restricted to certain parts of the bay such as Monterey Harbor and the bight located in the Northeast quadrant of the bay east of Santa Cruz. They also found that the Monterey Submarine Canyon (MSC) has a profound effect on the natural oscillations that occur within the bay. The canyon serves to separate the bay into two semi-independent halves with only weak coupling between them. Finally, periods were predicted for the lowest modes in Monterey Bay. The periods for the first 6 modes were 44.2, 29.6, 28.2, 23.3, 21.6, and 20.4 minutes. Separate predictions were made for Monterey Harbor with periods ranging from 1-2 minutes, to 13.3 minutes. Observational studies have consistently shown natural periods of oscillation for the bay of approximately 55, 36, 27, and 21 minutes (e.g., Lynch, 1970; Breaker et al., 2008), where an oscillation with a period of 55 minutes corresponds to the first longitudinal mode, and an oscillation with a period of 36 minutes corresponds to the first transverse mode.

Thus, it is the primary purpose of this study to compare the sea level response of these events in terms of their frequency content as recorded by the tide gauges in Monterey Harbor. However, where the data permit and sufficient supporting information exists, we examine other aspects of these events as well.

2. MATERIALS AND METHODS

Data Acquisition

In this section we provide background information on tidal measurements in Monterey Harbor and the tide gauges that were used to acquire water level data during the 1964 Great Alaskan Earthquake (GAE) and the 1989 Loma Prieta Earthquake (LPE).

On May 23, 1960, Prof. Warren Thompson of the U. S. Naval Postgraduate School in Monterey, California, recorded sea level fluctuations in Monterey Harbor, associated with a magnitude 8.5 earthquake that occurred off Chile. He noted seiches, or water level oscillations, that caused the sea level to rise and fall as much as six feet over a 20-minute period. Thompson was not able to witness the tsunami's arrival, but was able to record water level oscillations in the bay that occurred as a result of the initial perturbation (Berkman and Symons, 1964). This lead to an interest in recording tsunamis and other water level oscillations in southern Monterey Bay.

Thompson installed a Standard Tide Gauge in June 1963, which operated continuously until 1974.

The relatively simple Standard Gauge measures water levels directly through a system of pulleys and counterweights. It records water level on a strip chart or marigram, which is pulled forward by a clock mechanism. A float inside a protective well that extends at least a meter below the lowest anticipated tide level measures the water level. The standard opening at the bottom of the float well that is exposed to the ocean is reduced to 2 to 4 cm, to minimize interference by shorter wind waves. A pipe of the same inside diameter extends down 1.0 to 1.5 m below the orifice to reduce nonlinearities associated with higher frequency waves (Noye, 1974). The Standard Gauge records waves with periods from 30 to 60 seconds, to periods of several months (Bretschneider, 1983; Theberge, 2005). According to Cross (1967), the Standard Tide Gauge, similar to the one used by Thompson, "gives a good representation of tsunamis for periods larger than 5 minutes and wave heights of 2 feet (0.61 meters), or 15 minutes, for wave heights of 20 feet (6.1 meters)." We note that the periods and wave heights observed during this study did not exceed these limits.

In 1989, a Bubbler Tide Gauge was installed at Monterey according to the standards of NOAA's National Ocean Service (NOS). This gauge served as a backup for other tide gauges that were in operation at Monterey at that time. This instrument, which produced an analog record, was used to record the Loma Prieta earthquake during October 1989. Rabinovich et al. (1999) found that the dynamic response of the Bubbler Gauge, installed to NOS standards, is highly dependent on period, but for periods of roughly 10 minutes or greater, the response was 95-98% of the observed changes in water level. Thus, the response of this gauge was marginally sufficient to reproduce the 9-10 minute period oscillations that we observed during this event. Since the Bubbler Gauge produced an analog record, it allowed us to digitize the data at sufficiently high resolution to insure that the highest frequencies, as recorded by the instrument, were retained.

Data Preparation

For the GAE, paper records in the form of strip charts were obtained directly from the output of the tide gauge in Monterey Harbor for a period of approximately 72 hours starting several hours prior to the first arrival of this event. These strip charts were concatenated to produce a continuous 72-hour record. This record was next electronically scanned using a CONTEX FSC Model 5010, 36-inch Full Scale Color Scanner. A scanned record already existed for the tidal record at Monterey for the LPE. The scanned files were then imported into Photoshop where an image mask was applied and the original traces were isolated and assigned a color. Next, a program was written to import the traces into MATLAB and convert them into an RGB pixel image format. The image was then scanned to identify the trace in the MATLAB environment. Then information obtained from the original traces and from NOAA's Tide Tables was added to calibrate the records. The final step in each case was to digitize the traces at a resolution of 39 seconds between samples along the abscissa, and to less than one centimeter, along the ordinate. The first 5 hours were digitized in this manner for the LPE, and the first 47 hours for the GAE.

Singular Spectrum Analysis

Singular Spectrum Analysis (SSA) is based on a formal mathematical decomposition that consists of four steps. The first is the embedding step where a trajectory matrix is constructed from lagged versions of the original time series, second, a Singular Value Decomposition (SVD) of the matrix formed by the product of the trajectory matrix and its transpose, which corresponds to an eigenvalue problem that yields eigenvalues and eigenvectors, third, grouping, which involves splitting the matrices from the SVD into groups and summing the matrices within each group, and fourth, transforming the matrices into individual time series that can be summed to produce partial series, or if all of the individual series are summed, the original time series itself (e.g., Elsner and Tsonis, 1996; Golyandina et al., 2001). The method essentially decomposes the data into a set of independent modes where the user specifies the number of modes.

The embedding step can be accomplished by forming a trajectory matrix obtained from the time series, x_t, of length, N, where t =1, 2,....., N, as

$$\phi_{ij} = \frac{1}{N-L+1} \sum_{t=1}^{N-L+1} (x_{i+t-1} - \bar{x})(x_{j+t-1} - \bar{x}) \qquad (1)$$

L is the window length or embedding dimension and corresponds to the number of lagged vectors that are produced, each with dimension L, $1 \le i \le K$, where $K = N\text{-}L+1$, $1 \le j \le L$, and Φ_{ij} is the trajectory matrix whose dimensions are K x L. The mean value of the time series, , has been removed in each case prior to calculating Φ_{ij}.

A lagged-covariance matrix, $\tilde{M}$, is then formed from the trajectory matrix, Φ_{ij}, as follows

$$\tilde{M} = \frac{1}{K} \phi^T \phi \qquad (2)$$

where Φ^T is the transpose of Φ. From the second step above, SVD is applied to $\tilde{M}$ to extract the eigencomponents which include eigenvalues, eigenvectors, and the temporal principal components. When the square roots of the eigenvalues are plotted in descending order, we obtain the singular spectrum.

In conducting SSA, a suitable window length, L, must be chosen. L determines the number of lagged vectors that are used to form the trajectory matrix, and thus, the resolution of the decomposition. Values of L can vary from *2*, to $N-1$, but usually vary between *N/15* and *N/3* (Vautard, 1995). According to Golyandina et al. (2001), the choice of L depends on the application but should be large enough so that each L-lagged vector includes an essential part of the behavior of the system. As a rule, L is usually varied over a range of values before a final value is chosen, but experience with the method and familiarity with the data are extremely helpful in making this choice.

3. RESULTS

Loma Prieta Earthquake of 1989

On October 18, 1989 at 0104 GMT, a surface-wave magnitude 7.1 earthquake occurred on the San Andreas fault in the Santa Cruz Mountains approximately 16 km northeast of Santa Cruz, California (McNutt, 1990). The corresponding seismic moment for this event was 6.9 on the moment magnitude scale. Consistent with this general description, a tsunami was generated that propagated across at least part of the bay, arriving at the tide gauge in Monterey Harbor approximately 20 minutes after the main event (Schwing et al., 1990). However, from the various reports that appeared following the Loma Prieta earthquake it is not exactly clear where and how the tsunami was generated. According to Schwing et al. (1990), and Gardner-Taggert and Barminski (1991), the tsunami may have been caused by vertical uplift from the initial shock wave at the coast near Santa Cruz. However, subsequent observations in Monterey Submarine Canyon indicate that this earthquake produced offshore landslides along the walls of the canyon (Gardner-Taggert and Barminski, 1991), slumping along the south wall of the canyon (Greene et al., 1991), and turbidity currents (Garfield et al., 1994), processes that each could have generated a tsunami. Ma et al. (1990) produced a synthetic tsunami for the bay based on the seismic characteristics of the earthquake and concluded that large-scale slumping near Moss Landing could have generated a tsunami similar to that observed at Monterey. It is possible, and perhaps likely, that more than one process contributed to the observed sea level response at Monterey. The height of a tsunami can be roughly estimated near the source of generation according to

$$\mathrm{Log}_{10}H = 0.75M - 5.07 \qquad (3)$$

where H is the wave height in meters and M is the Richter or surface-wave magnitude (e.g., Camfield, 1980). However, this empirical relationship does not completely take into account the characteristics of the generating mechanism or the coastline. Also, we prefer to use the moment magnitude instead of the surface-wave magnitude because of its improved physical basis including the fact that it does not tend to saturate at higher magnitudes (e.g., Bryant, 2001). However, as we shall see in the following section, using the moment magnitude instead of the surface-wave magnitude does not always produce better results. Using (3), with a value for M of 6.9, we obtain a value of 1.3 meters for the LPE. The period of a tsunami can be estimated according to

$$\mathrm{Log}_{10}T = 0.625M - 3.31 \qquad (4)$$

(Wilson and Torum, 1968), where T is the period in minutes and M is the magnitude. In this case, we obtain a period of 10.1 minutes. Estimates of the amplitude and period of this event provide a basis for comparison with the observed sea level response at Monterey.

In the top panel of Fig. 2 (Fig. 2a), the tide gauge record for the three-day period from 17-20 October 1989 is shown. In the lower panel (Fig. 2b) we have extracted a 5-hour segment of this record for closer inspection. The primary response to this event appears to have taken

place during the first 15 hours or so after t_0 (the first arrival of the event), although weaker indications could be observed in the record for up to 3 days. Following the main event, the two largest aftershocks were of magnitude 5.2 and 5.0 on the Richter scale (McNutt, 1990), and so were not sufficient to generate additional tsunamis (e.g., Wilson et al., 1962). According to Murty et al. (2006) and Murty et al. (2008), the influence of tsunamis can last for several days due to arrivals from the same event that have taken multiple paths through reflections, energy trapping, and secondary undulations.

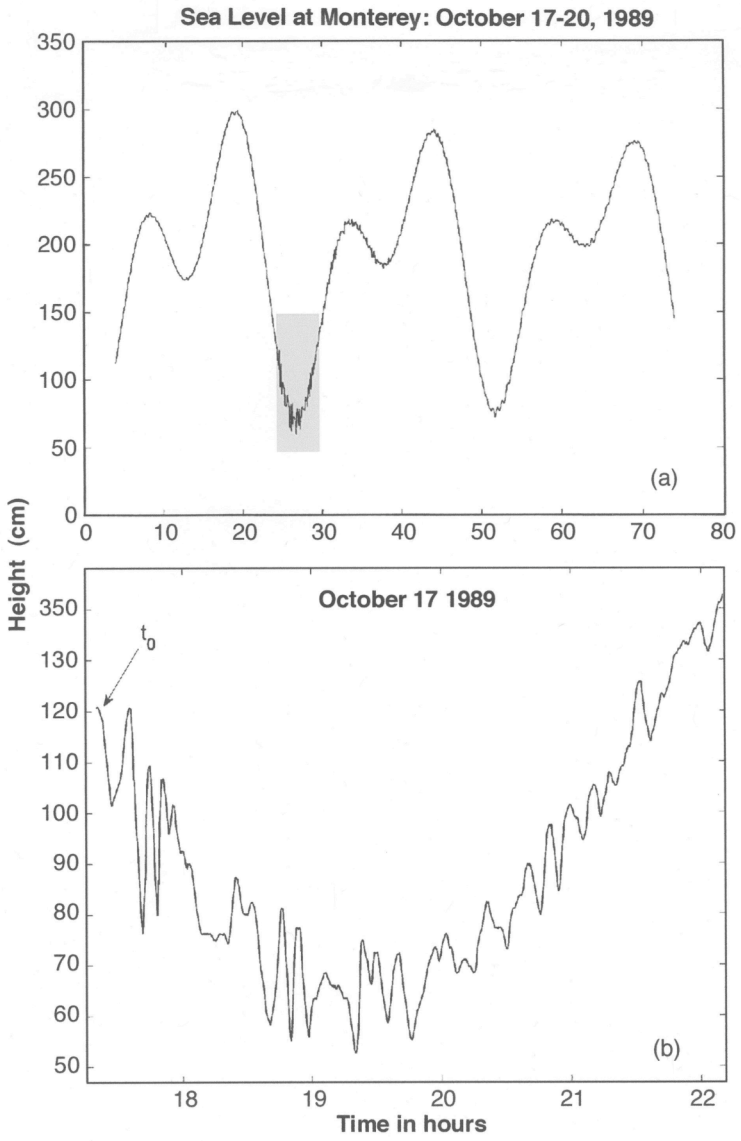

Figure 2. The top panel, (a), shows a segment of the tidal record at Monterey during the period of the LPE from 17 to 20 October 1989. The area shaded in gray corresponds to the first five hours of this event. The lower panel, (b), shows the first five hours in greater detail where t_0 indicates the first arrival of this event.

The apparent maximum range of variability during the period shown in Fig. 2b is of the order of 45 cm. However, due to the response characteristics of the tide gauge employed and the subsequent data processing, this record may underestimate the true amplitude of the signal, significantly. If our estimate of the initial wave height (1.3 meters) is realistic, then a maximum observed range of 45 cm is smaller than the predicted wave height by almost a factor of 3.

Singular Spectrum Analysis (SSA) has been applied to the record shown in Fig. 3b in order to extract the primary frequencies contained therein. The eigenvalues in Fig. 3a show how the variance is partitioned by mode. A window length, *L*, of 300 (3.25 hours) was chosen.

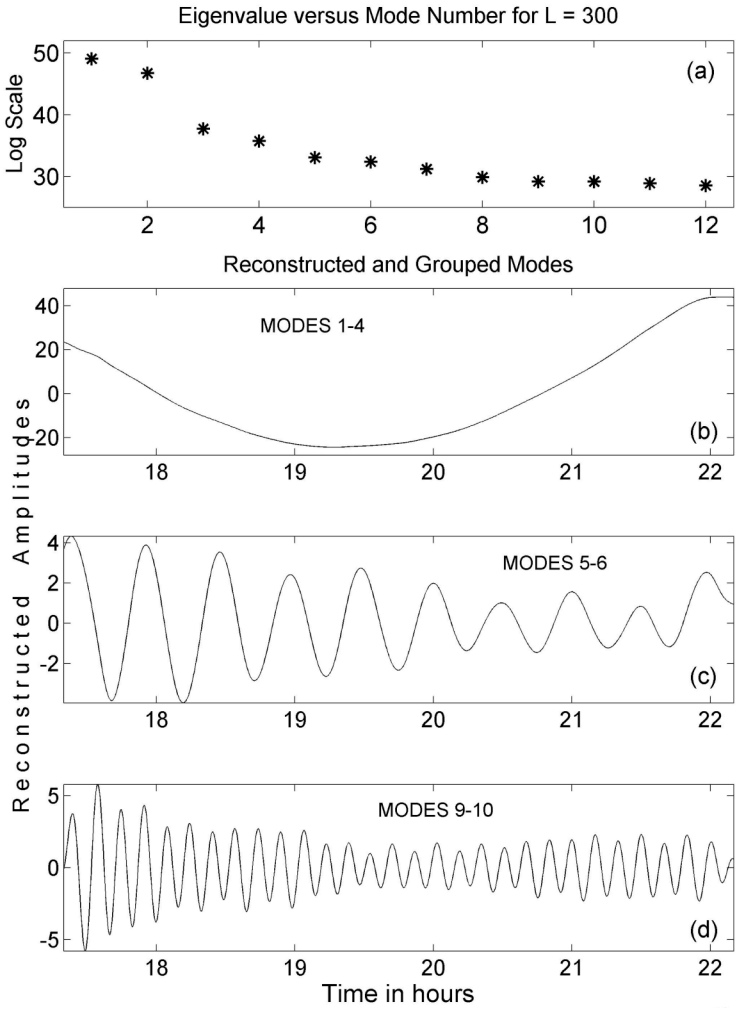

Figure 3. The top panel, (a), shows the distribution of eigenvalues for the first 12 modes of the singular spectrum analysis for the record shown in Fig. 2b, for a window length of 300 (3.25 hours). The scale on the vertical axis is logarithmic. The second panel, (b), shows the first four reconstructed modes which correspond to the astronomical tide. The third panel, (c), shows reconstructed modes 5 and 6, which reveal an oscillation with a period of 31-32 minutes, and the bottom panel, (d), shows reconstructed modes 9 and 10, which reveal an oscillation with a period of 9-10 minutes.

The first 4 modes account for 88.6%, and the first 10 modes, 93.6%, of the total variance. When the first four modes are reconstructed and grouped, they closely approximate the underlying tidal signal (Fig. 3b). When modes 5 and 6 are combined (Fig. 3c), they correspond to an oscillation with a period of 31-32 minutes. Again, this period is not fixed, but varies slightly. A period of 31-32 approaches the expected period of transverse oscillation for the bay. The transverse mode as described by Wilson et al. (1965) has a nodal line across the entrance of the bay and an antinode at Moss Landing (Fig. 1). The expected period is approximately 36 minutes and has been observed on a number of occasions, and, again, as we shall see, after we examine the GAE. Modes 9 and 10, taken together (Fig. 3d), reproduce an oscillation with a period of 9-10 minutes, consistent with the findings of Schwing et al. (1990). This oscillation does not represent a pure tone, but, rather, one whose period varies slightly, i.e., it is frequency modulated. The period is close to the predicted period of the tsunami itself which was 10.1 minutes. However, it is likely that the tsunami associated with the LPE was at least partially influenced by the boundaries of the bay when it arrived at Monterey Harbor and so its frequency content may have been altered as it propagated south and began to take on the characteristics of a seiche. Finally, a period of 9-10 minutes falls well within the range of seiche periods for Monterey Harbor as predicted by Wilson et al. (1965).

The Great Alaskan Earthquake of 1964

On March 28, 1964 at 03:36 GMT, a shallow earthquake of surface-wave magnitude 8.3 and a moment magnitude of 9.2 occurred at 61.0°N, 147.8°W in Prince William Sound, in south-central Alaska (Page, 1968). Uplifting caused vertical displacements as large as 16 m on the sea floor in the vicinity of the epicenter (Malloy, 1964). According to Plafker and Mayo (1965), submarine uplift of the continental shelf within Prince William Sound and considerably beyond, generated a train of long-period large-amplitude seismic sea waves, or tsunamis, that were recorded at tide gauges throughout the Pacific basin. The tsunami that was generated by this earthquake propagated across the Pacific basin and south along the west coast of North America reaching the latitude of Monterey Bay at approximately 08:18 GMT on March 28, 1964. During the first day following the main event there were 11 aftershocks of surface-wave magnitude 6.0, or greater (Page, 1968), but none large enough to generate a second tsunami.

Cylindrically symmetrical dispersive waves decay approximately according to $1/r$, where r is the distance from the epicenter, and the effects of bottom depth are not taken into account. However, when the tsunami approaches the coast the effects of bottom depth must be taken into account, and both refraction and dispersion may become important. Thus, without the help of a numerical model that contains the governing physics and the appropriate initial and boundary conditions, it is not a simple matter to estimate the height of the tsunami when it reached Monterey Bay. Since the period remains essentially constant we can estimate this parameter, and using equation (4) with a magnitude of 8.3, we obtain a value of 75.4 minutes. This value is very close (a difference of less than 1 minute) to the period of positive surge observed at Wake Island following the GAE (Van Dorn, 1964). We note that using a moment magnitude of 9.2 in this case predicts a period of almost 4.6 hours which is far greater than the period that was observed for this event.

Fig. 4a shows a digitized version of the strip chart that was originally recorded from the tide gauge in Monterey Harbor for the two-day period (actually, 47 hours) following the first arrival of this event at t_0. In Fig. 4b, we have extracted a 5-hour portion of the record. The peak-to-trough range of the oscillations associated with this event approach, or even exceed, 100 cm, rivaling the amplitude of the semidiurnal tide itself. Over the first two days, the amplitudes of the oscillations associated with this event decrease by roughly an order-of-magnitude. However, oscillatory behavior could be detected for at least four days following the main event, due to multipath effects, which spread the arrival pattern over time.

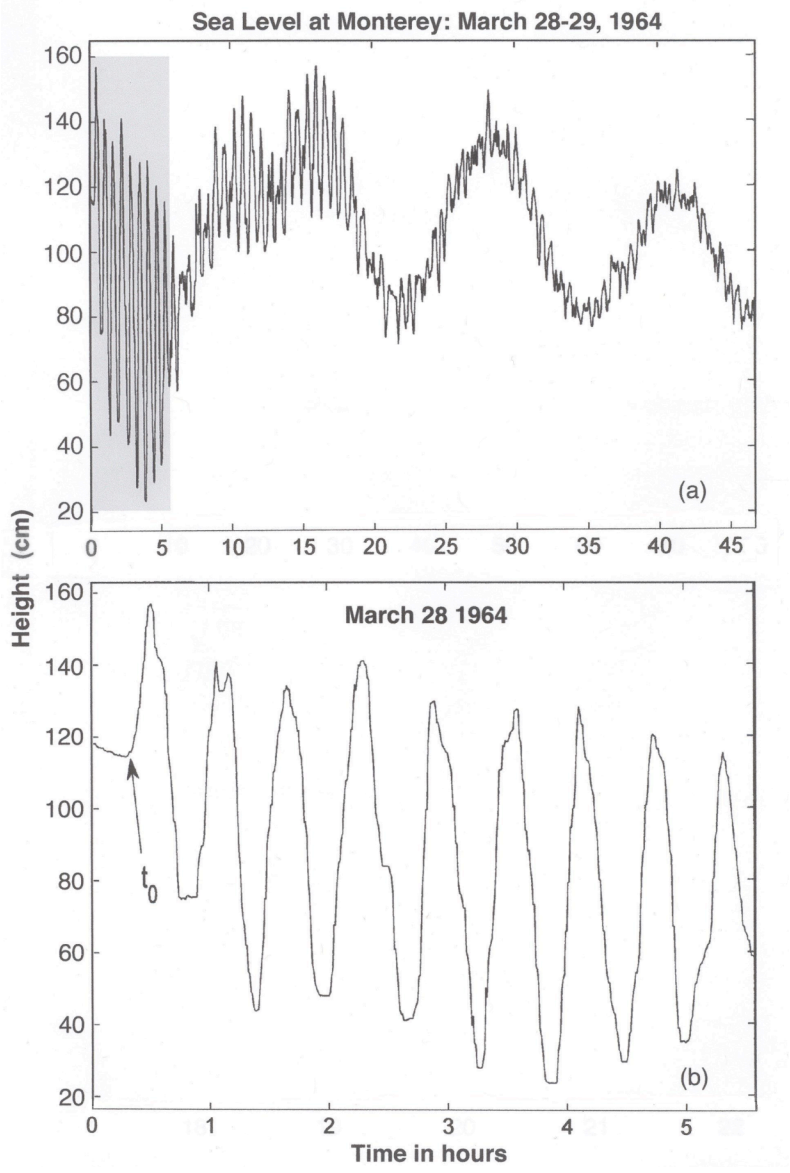

Figure 4. The top panel, (a), shows a segment of the tidal record at Monterey during the period of the GAE from 28 to 29 March 1964. The area shaded in gray corresponds to the first five hours of this event. The lower panel, (b), shows the first five hours in greater detail where t_0, again, indicates the first arrival of this event.

An examination of the record in Fig. 4a shows that two bursts of 6 or 7 oscillations followed within 2-3 hours of the initial burst, which consists of 10 oscillations. After the first 20 hours, the oscillations continue but are no longer burst-like. They are more continuous in nature with amplitudes that gradually decrease with time. This trend continues out to four days at which time the oscillations were barely detectable (not shown). The second two bursts that follow the initial burst suggest that they could be due to reflections that occurred relatively close to the epicenter because of their similarity to the initial burst. Because there are no obvious reflecting boundaries outside Monterey Bay for great distances it is unclear how reflections could play a significant role in contributing to these secondary oscillations unless they occurred much closer to the epicenter. The initial disturbance could have been reflected from bathymetric features along the Aleutian Chain as it spread southward from the epicenter. However, without detailed calculations that take into account the possible propagation paths that could have produced arrival times matching those in the record, we cannot answer this question. Thus, we also consider energy trapping and secondary undulations as processes that may have contributed to the extended oscillations. Energy trapping can take the form of continental shelf waves that are trapped over the continental margin by the sloping bottom and are strongly influenced by the earth's rotation. However, because these waves are generated and propagate along the open coast it is unlikely that they are responsible for the extended oscillations observed in the tide gauge record at Monterey. Energy trapping can also generate infragravity waves called edge waves, which appear to have been previously observed in Monterey Bay (MacMahan et al., 2004a; MacMahan et al., 2004b). Yanuma and Tsuji (1998) showed that using a shelf slope of 1/1000 and a shelf width of 1 km, a period of approximately 27 minutes is predicted for the first standing edge wave mode. In the shallow shelf regions of Monterey Bay, away from MSC, edge waves with periods of the same order are predicted.

According to Kowalik and Murty (1993), secondary undulations are oscillations whose periods correspond to the normal modes of the bay and can be excited by a number of different sources, including tsunamis. These secondary undulations can be classified rather generally as one of three types, A, B, or C, depending on the geometry of the bay (Nakano, 1932). In type A, the secondary undulations appear as coherent wave trains with approximately the same waveform. In type B, they are not as regular and coherent as in type A, but are not completely irregular. In type C, they are essentially irregular in form. The type of secondary undulations can be roughly determined by plotting the depth of the bay versus $10S/b^2$, where S corresponds to the surface area of the bay and b is its breadth. For Monterey Bay, with a surface area, S, of roughly 800 km^2, a breadth of approximately 20 km, and an average depth of 100m, we find that secondary undulations fall into category B, where they are not as regular and coherent as in type A, but are not completely irregular. On a qualitative basis, we find this result is generally consistent with the oscillatory patterns exhibited in the record. In summary, although the pair of secondary bursts between hours 8 and 18 in Fig. 4a may be due to reflections, we are not able to identify any reflecting boundary near Monterey Bay that may have been responsible. Both edge waves and secondary undulations inside the bay provide reasonable explanations for the observed pattern of oscillations that lasted for up to 4 days following the initial burst.

We have applied SSA to this record as well. Fig. 5a shows the first 10 eigenvalues, which account for over 90% of the total variance. A window length of 1000 or 10.8 hours was used,

which is about 23% of the record length. When the first three modes are reconstructed and grouped (Fig. 5b), they approximately represent the predicted semidiurnal tide, at least for the last two cycles.

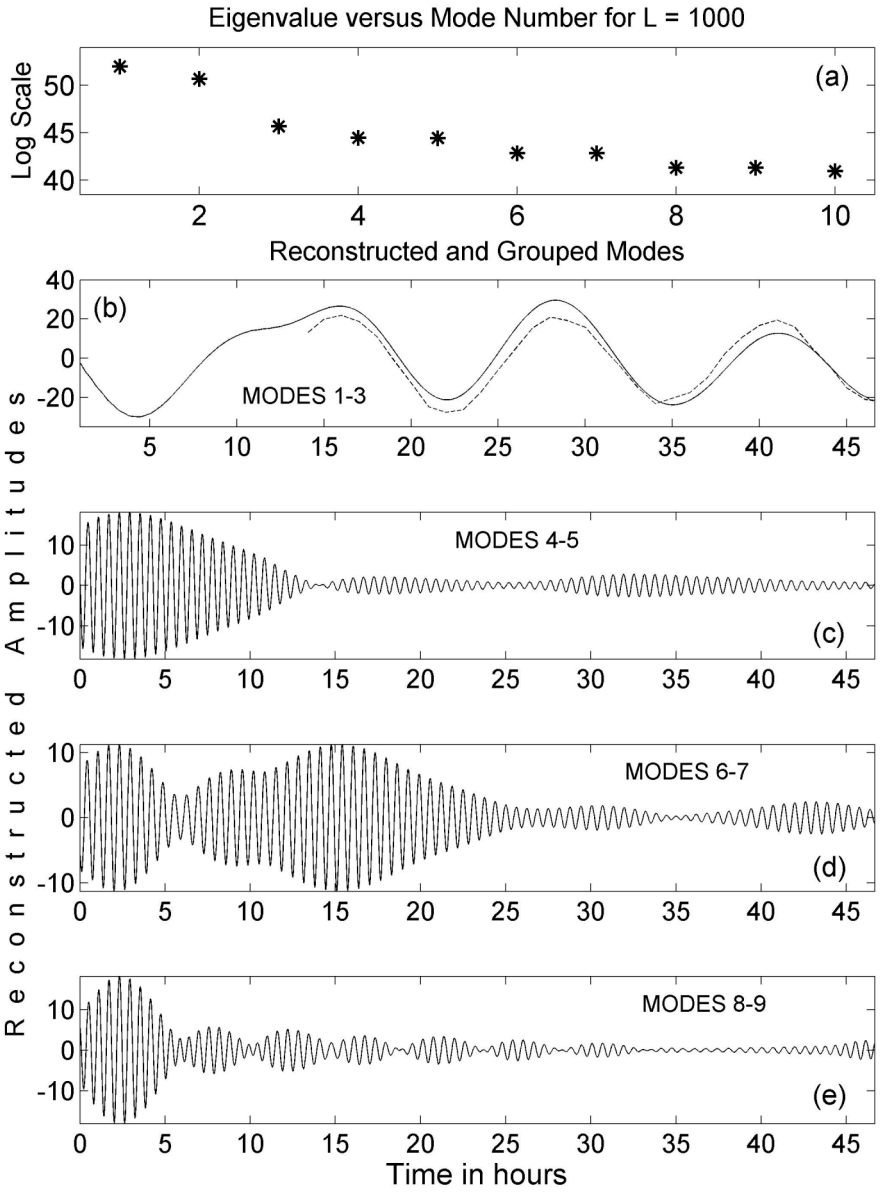

Figure 5. The top panel, (a), shows the distribution of eigenvalues for the first 10 modes of the singular spectrum analysis for the record shown in Fig. 4, for a window length of 1000 (10.8 hours). The second panel, (b), shows the first three reconstructed modes, which correspond to the astronomical tide. The dashed line shows the corresponding semidiurnal tide from the NOAA Tide Tables for 1964. The third panel, (c), shows reconstructed modes 4 and 5, the fourth panel, (d), reconstructed modes 6 and 7, and the fifth or bottom panel, (e), reconstructed modes 8 and 9. The period in each case is approximately 37 minutes.

During the first 10-15 hours, nonlinear interaction between the tidal signal and the tsunami-driven seiche may have occurred, leading to distortion in the observed waveform. When modes 4 and 5, 6 and 7, and 8 and 9 are reconstructed and grouped, they each have a period of approximately 37 minutes, ±0.5 minutes. Each grouping appears to represent a different aspect of the same oscillation, most likely, separate arrivals that occurred during the period of observation. An observed oscillation with a period of approximately 37 minutes is in close agreement with the past observations of Lynch (1970) and Breaker et al. (2008). A period of 37 minutes corresponds closely to the expected transverse mode of oscillation for the bay that assumes a nodal line across the entrance from the Monterey Peninsula to Santa Cruz (Fig. 1). This mode of oscillation is consistent with a tidal wave that enters the bay from the west. As the wave conforms to the bay's dimensions, it is transformed into a seiche whose period has often been observed, and at least approximately predicted by Wilson et al. (1965). We also note that a period of 37 minutes corresponds to a frequency that is approximately twice the frequency associated with the period of the 1964 tsunami, which was about 75 minutes. This raises the question of resonance between the incoming tsunami and the corresponding seiche it produced. If we consider the case of harbor resonance, as described by LeBlond and Mysak (1988), where the wave motion is excited by forcing at the entrance, the response may be expressed as the ratio of the maximum amplitude inside the harbor to the amplitude at the entrance. The simplest case of a resonant response occurs for quarter-wave resonance. In this case the only processes that limit the amplitude inside the harbor are dissipative in nature. In harbors where this happens, the entrance corresponds to a nodal line and the antinode occurs at a distance of one-quarter wavelength inside the harbor (Fig. 1). This appears to be the same situation that has occurred in Monterey Bay with respect to the GAE. And since the resonant frequency of the bay for the transverse mode is almost an integer multiple of the forcing frequency, the opportunity for resonant interaction to occur may have been enhanced. Finally, although the groupings for modes 4 and 5, 6 and 7, and 8 and 9 are independent, each represents the same frequency, a result that we have not previously encountered in the application of SSA.

4. CONCLUSIONS

Singular Spectrum Analysis (SSA) was particularly effective in extracting the primary frequencies associated with each event, consistent with the findings and recommendations of Golyandina et al. (2001), and Ghil et al. (2002). It is not clear how or exactly where the tsunami associated with the 1989 Loma Prieta Earthquake (LPE) was generated in Monterey Bay, although these questions have been discussed in the literature. It may have been initiated at the north end of the bay near Santa Cruz, along the south wall of Monterey Submarine Canyon, or further up the canyon near Moss Landing. It is most likely that the tsunami generated by the LPE began to take on the characteristics of a seiche by the time it reached the tide gauge in Monterey Harbor. Our results indicate that the LPE was responsible for generating one mode of oscillation with a period of 9-10 minutes, generally consistent with the predicted periods of oscillation for Monterey Harbor, and a second oscillation with a period of 31-32 minutes that most likely corresponds to a bay-wide oscillation.

The initial peak-to-trough amplitude of the sea level response to the GAE was close to 100 cm and thus of the same order as the amplitude of the semidiurnal tide itself. Two bursts of 6-7 oscillations followed within 2 to 3 hours after the initial burst of 10 oscillations and may have been due to reflections of the main event and thus taken a slightly longer path on their way across the Pacific. We conclude that edge waves and secondary undulations may have also contributed to the oscillatory behavior observed in the sea level record out to a period of almost 4 days. SSA revealed oscillations with a period of approximately 37 minutes, which corresponds to the transverse mode of oscillation that has previously been observed. Although different arrivals were included in the SSA decomposition, only a single frequency with a period of ~37 minutes was found, consistent with a strongly resonant response. This mode of oscillation is consistent with a tidal wave that entered the bay from the west where a nodal line extends across the entrance from the Monterey Peninsula to Santa Cruz. We conclude that the tsunami produced quarter-wave resonance within the bay consistent with the observed seiche-like response in sea level.

The sea level responses to the LPE and the GAE were entirely different, not only because of the large difference in the magnitudes of these events, but also because the driving force in one case occurred inside the bay (LPE), and in the second, outside the bay (GAE). As a result, different modes of oscillation were excited.

5. ACKNOWLEDGMENTS

Charlie Endris from Moss Landing Marine Laboratories is thanked for helping us to scan the original strip chart record for the Great Alaskan Earthquake of 1964.

6. REFERENCES

Berkman. S.C. and J.M. Symons, (1964). The tsunami of May 22, 1960 as recorded at tide stations. U.S. Department of Commerce, Coast and Geodetic Survey, Washington 25, D.C., 69pp.

Bretschneider, D., (1983). Sea level variations at Monterey, CA, U.S. Dept. Commer. NOAA Tech. Rep. NMFS SSRF-761, 50 pp.

Bryant, E., (2001). TSUNAMI: The Underrated Hazard. Cambridge University Press, Cambridge, UK.

Camfield, F.E., (1980). Tsunami Engineering. Special Report No. 6. U.S. Army, Corps of Engineers, Coastal Engineering Research Center, Fort Belvoir, VA, 222 pp.

Cross, R. H., (1967). Frequency response of tide gages. University of California, Berkeley, Hydraulic Engineering Laboratory, Technical Reports HEL, 16 - 2,3,4.

Elsner, J.B. and A.A. Tsonis, (1996). Singular Spectrum Analysis: A New Tool in Time Series Analysis. Plenum Press, New York and London.

Gardner-Taggart, J.M. and R.F. Barminski, (1991). Short period wave generation in Moss Landing harbor caused by offshore landslides induced by the Loma Prieta earthquake. Geophysical Research Letters, 18, 1277-1280.

Garfield, N., T.A. Rago, K.J. Schnebele, and C.A. Collins, (1994). Evidence of a turbidity current in Monterey Submarine Canyon associated with the 1989 Loma Prieta earthquake. Continental Shelf Research, 14, 673 - 686.

Ghil, M., M.R. M.D. Allen, K. Dettinger, D. Kondrashow, M.E. Mann, A.W. Robertson, A. Saunders, Y.Tian, F. Varadi, and P.Yiou, (2002). Advanced spectral methods for climatic time series. Reviews of Geophysics, 40, 1003, 3-1 – 3-41.

Gohres, H., (1964). Tidal Marigrams, San Diego Historical Society Quarterly. October 1964, 10 (4), http://www.sandiegohistory.org/journal/64october/marigram.htm.

Golyandina, N., V. Nekrutkin and A. Zhigljavsky, (2001). Analysis of Time Series Structure: SSA and Related Techniques. Monographs on Statistics and Applied Probability 90. Chapman & Hall/CRC, Boca Raton.

Greene, H.G., J. Gardner-Taggart, M.T. Ledbetter, R. Barminski, T.E. Chase, K.R. Hicks and C. Baxter, (1991). Offshore and onshore liquefaction at Moss Landing spit, central California - result of the October 17, 1989, Loma Prieta earthquake. Geology, 19, 945 - 949.

Kowalik, Z., and T.S. Murty, (1993). Numerical Modeling of Ocean Dynamics. World Scientific, Singapore.

LeBlond, P.H. and L.A. Mysak, (1978). Waves in the Ocean. Elsevier Oceanography Series 20. Elsevier Scientific Publishing Company, Amsterdam.

Ma, K., K. Sataki and H. Kanamori, (1990). Tsunami of the 1989 Loma Prieta earthquake (abstract). EOS Transactions AGU, 71, pp. 1460.

MacMahan, J.H., J.H. Reniers, E.B. Thornton and T.P. Stanton, (2004a). Infragravity rip current pulsations. Journal of Geophysical Research, 109, C01033, doi: 10.1029/2003JC002068.

MacMahan, J.H., J.H. Reniers, E.B. Thornton and T.P. Stanton, (2004b). Surf zone eddies coupled with rip current morphology. Journal of Geophysical Research, 109, C07004, doi: 10.1029/2003JC002083.

Malloy, R.J., (1964). Crustal uplift southwest of Montague Island, Alaska. Science, 146, 1048-1049.

McNutt, S., (1990). Loma Prieta earthquake, October 17, 1989. California Geology, 43, 3 - 7.

Murty, T.S., (1977). Seismic Sea Waves: Tsunamis. Bulletin of the Fisheries Research Board of Canada, Bulletin 198, Ottawa, Canada.

Murty, T.S., N.P. Kurian, and M. Baba, (2006). Trans-oceanic reflection of tsunamis: the Kerala example. Disaster & Development, 1, 65 - 76.

Murty, T.S., N.P. Kurian, and M. Baba, (2008). Roles of reflection, energy, trapping and secondary undulations in the tsunami on Kerala coast. International Journal of Ecology & Development, 10, 100-114.

Nakano, M., (1932). Preliminary note on the accumulation and dissipation of the energy of secondary undulations in a bay. Proc. Phys. Math. Soc. Japan, SER 3, 44-56.

Noye, B.J., (1974). Tide-well systems II: the frequency response of linear tide-well system. Journal of Marine Research, 32, 155 -181.

Page, R., (1968). Aftershocks and microaftershocks of the Great Alaska Earthquake of 1964. Bulletin of the Seismological Society of America, 58, 1131-1168.

Plafker, G. and L.R. Mayo, (1965). Tectonic deformation, subaqueous slides and destructive waves associated with the Alaskan March 27, 1964 earthquake. Open File Report, U.S. Geological Survey, Menlo Park, CA, 19 pp.

Rabinovich, A.B., R.E.Thomson, E.A. Kulikov, B.D.Bornhold and I. V. Fine, (1999). The landslide-generated tsunami of November 3, 1994 in Skagway Harbor, Alaska: A case study. Geophysical Research Letters, 26, 3009 -3012.

Schwing, F.B., J.G. Norton and C.H. Pilskaln, (1990). Earthquake and bay response of Monterey Bay to the Loma Prieta earthquake. EOS Transactions of the American Geophysical Union, 71, 250-251, 262.

Theberge, A.E., (2005). 150 years of tides on the western coast, the longest series of tidal observations in the Americas. Center for Operational Oceanographic Products and Services, National Ocean Service, NOAA, DOC, Washington, D.C., 15 pp. http://co-ops.nos.noaa.gov/publications/150_years_of_tides.pdf

Van Dorn, W.G., (1964). Source mechanism of the tsunami of March 28, 1964 in Alaska. Proceedings of the Ninth Conference on Coastal Engineering, American Society of Civil Engineers, Chap. 10, 166-190.

Vautard, R., (1995). Patterns in time: SSA and MSSA. In: von Storch, H., Navarra, A. (Eds.), Analysis of Climate Variability: Applications of Statistical Techniques. Springer-Verlag, Berlin, pp. 259-279.

Wilson, B.W., L.M. Webb and J.A. Hendrickson, (1962). The nature of tsunamis: their generation, and dispersion in water of finite depth. Technical Report no. SN 57-2, National Engineering Science Company, 150 pp.

Wilson, B.W. and A. Torum, (1968). The tsunami of the Alaskan earthquake, 1964: engineering evaluation. TM-25, U.S. Army Coastal Engineering Research Center, Washington, D.C.

Yanuma, T. and Y. Tsuji, (1998). Observations of edge waves trapped on the continental shelf in the vicinity of Makurazaki Harbour, Kyushu, Japan. Jour. Oceanog., 54, 9-18.

REVIEW OF RECONSTRUCTION IN ACEH FOLLOWING THE 2004 BOXING DAY TSUNAMI

Zygmunt Lubkowski[1], Jo da Silva[2], Kubilay Hicyilmaz[3] and Damian Grant[4]

[1] *Associate Director, Arup International Development, London, UK*
[2] *Director, Arup International Development, London, UK*
[3] *Senior Engineer, Arup International Development, Dubai, UAE*
[4] *Engineer, Arup International Development, New York, USA*
Email: zygi.lubkowski@arup.com

ABSTRACT

This paper summarises the findings of two field trips to the Aceh Province, which were made by the authors, in early 2006 and late 2007. The purpose of the trips was to assess and provide guidance to the rebuilding process following the 26 December 2004 earthquake and tsunami. The paper will discuss the key issues raised and show how the various agencies involved in the rebuilding process have met the challenges encountered.

KEYWORDS: Aceh, Tsunami, Disaster Risk Reduction, Reconstruction

1. INTRODUCTION

The Indian Ocean earthquake that occurred at 07:58:33 local time on the 26 December 2004, originated just north of Simeulue Island, off the western coast of northern Sumatra, Indonesia. The earthquake triggered a series of tsunamis that spread throughout the Indian Ocean, killing large numbers of people and devastating coastal communities in Indonesia, Sri Lanka, India, Thailand, and as far a field as Somalia. Aceh, in Northern Indonesia, was the worst hit region where it is estimated some 170,000 people died, and numerous buildings and infrastructure were completely destroyed, leaving more than 500,000 people without homes, access to water and sanitation, and livelihoods. A second major earthquake on 28 March 2005, with its epicentre north of Nias caused further loss of life and damage.

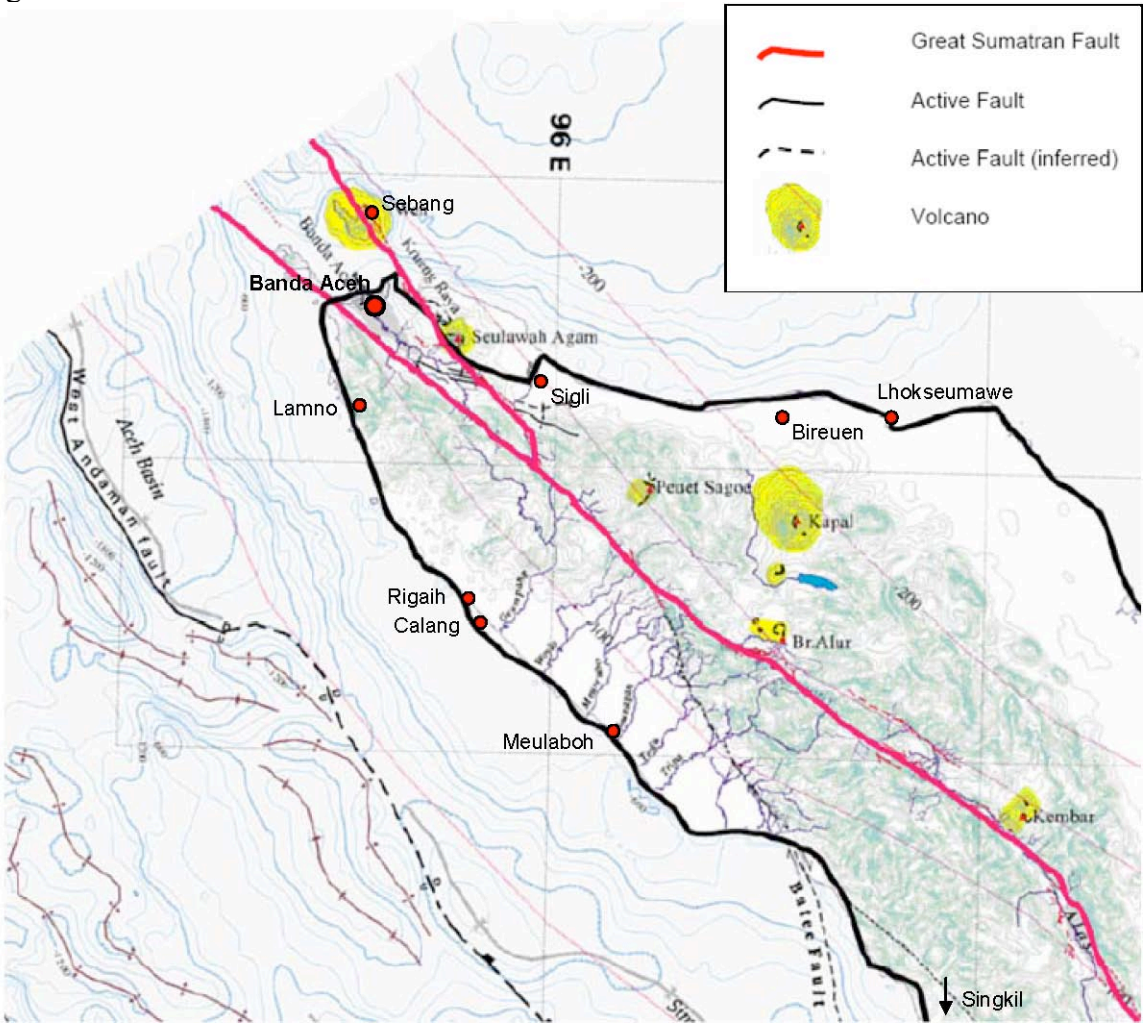

Figure 1 Principal Locations and Geological Features of the Aceh Province

This paper presents the findings of two field trips to the Aceh Province. The purpose of the initial trip, in early 2006, was to carry out a technical review of the existing construction programme of the NGO Muslim Aid, in order to assess the adequacy of their structures. As a consequence of the information gathered during the trip we also provided key findings to UN agencies and other NGOs so that these could benefit all parties and the wider reconstruction effort. The second trip, in late 2007, looked at reviewing the achievements made by various organizations involved in the rebuilding process. This paper also provides recommendations for the ongoing process in Aceh and future earthquake reconstruction and disaster risk reduction projects in developing regions.

The focus of the trips was on the construction of rural housing, water and sanitation, schools and health centres. For the purpose of this paper we shall concentrate purely on the rural housing and water and sanitation issues, though many of the observations apply to all forms of construction.

Figure 1 shows the Aceh region and identifies the principal locations that were visited during the two visits, from Singkil on the south west coast to Lhokseumawe on the north east coast of Aceh. Each trip covered more than 1000km of the Aceh coastline.

We would like to thank all the people and organisations who gave up their precious time to meet and discuss their respective projects and in particular Fadullah Wilmot the Country Director for Muslim Aid.

2. NATURAL HAZARDS

One of the key issues identified was a lack of understanding of the various natural hazards which could affect Aceh. Many of the parties involved in the re-construction process were focused on protecting against another tsunami, to the detriment of other potentially more important concerns (see Figure 1).

This paper does not present a once and for all authoritative list of all natural hazards relevant to Aceh, rather we hope to show the need for a holistic assessment of natural hazards and so provide an insight into the difficult balances that need to be struck between available location for building, economic means to engineer against and methods of managing the implications of the various natural hazards.

In an ever increasingly populated world due care and attention must also be given to man made hazards and sustainability principles to ensure that any building process is properly understood in its entirety and appropriate strategies to handle the situation are decided upon.

2.1 Tectonic Setting

Sumatra lies just to the east of the Sunda Trench and delineates the subduction of the Indian and Australian Plates below the Sunda Plate. Aceh province lies at the apex of this junction. This tectonic collision zone has given rise to the mountain range along the spine of Sumatra and the numerous volcanoes, earthquakes and tsunamis that have characterised the geological history of the region.

2.2 Volcanoes

Most of Indonesia's volcanoes lie along the Sunda arc. Data on the current activity of volcanoes can be obtained from the Volcanological Survey of Indonesia (see http://www.vsi.esdm.go.id/), whilst a list of active volcanoes in Aceh can be found at the following web site: http://www.volcano.si.edu.

Since the probability of a major event may be very small, it often proves neither politically nor economically viable to prohibit building within the volcano eruption risk zone. Neither is it practical to design structures for pyroclastic eruptions. Instead, monitoring of potentially active volcanoes, such as Seulawah Agam, and the design, training and implementation of evacuation plans, can ensure that future lives are saved. Structures outside the most hazardous zones will be affected by ash fall from eruptions. It is therefore important to consider the additional weight of ash when designing roofs.

2.3 Tsunami

Indonesia has a long history of damaging tsunamis, which have been caused by earthquakes and volcanic eruptions. Other non-seismic events, such as a landslides, man-made explosions and meteorite impact can also generate a tsunami. Information on historic tsunamis that have affected Sumatra can be found at: http://www.ngdc.noaa.gov/.

Designing structures for tsunami with water heights of more than a couple of metres is both difficult to achieve and costly. One possible solution is therefore to locate structures away from exposed coastline areas. However, local economics and social needs dictate that people will tend to relocate back to where they lived previously. For a small more common event, the combination of planting and landscaping of the coastline can be used to protect vulnerable communities. Wherever possible, housing should be built away from the sea on higher level ground to mitigate a tsunami risk.

For a large rare event, tsunami warning systems have been shown to work effectively in both Japan and Hawaii. However, for such systems to be effective they require suitable evacuation routes to be provided together with an extensive education program. This will ensure the population at risk will be able to self-evacuate prior to any future event. Unfortunately in Aceh houses are being constructed on an individual basis rather than as part of an integrated urban plan that facilitates provision of evacuation routes.

2.4 Earthquakes

Major earthquakes that have affected Sumatra over the last two centuries are generated either along the Sunda Trench in the Indian Ocean or from the Sumatran fault, which runs the length of Sumatra.

Earthquakes on the Sunda Trench are generated by the subduction process. These are amongst the world's largest earthquakes. There is a general academic consensus (McClosky et al., 2005, Sieh, 2005 and Nalbant et al., 2005) that there is now an increased risk that the next part of the subduction zone to the south will rupture in the next few years.

Earthquakes on the Sumatran Fault are generated by the strike slip motion along that fault. It is interesting to note that the Aceh segment has no recorded rupture in the last century, which may

suggest that an earthquake may be imminent. Furthermore, McClosky et al. (2005), Sieh (2005) and Nalbant et al. (2005) all raise concern that segments of the Sumatran Fault closest to the 26 December 2004 and 28 March 2005 events might also be triggered by the changes in stress associated with these large events.

It should be noted that any earthquake induced rupture along the Sunda Trench would be at least 100km from Banda Aceh, whilst an earthquake rupture on the Aceh section of the Sumatran Fault could be less than 10km away. As a result, the ground motion and hence damage due to the more local event could potentially be more significant even though the magnitude of an earthquake along the Sunda Trench is larger.

2.5 Other Hazards

2.5.1 Wind

Aceh Province lies just to the south of the tropical storm belt however it is still subject to relatively high prevailing winds. Appropriate design to the latest structural codes and competent construction should ensure adequate structural performance of buildings.

2.5.2 Flooding (Rainfall)

The average rainfall for Banda Aceh is about 1.6m in a year, with the principal rainy season being between September and January. The region is therefore susceptible to large water run-off that can lead to flash flooding. This requires adequate drainage design. Locating housing on high ground, or elevating it on stilts reduces the impact of flooding. Where developments are to be built on or near slopes, it is important that terraces and drainage channels are sufficiently engineered to ensure their stability (Figure 2a).

The cost of properly designed engineering works to create suitable sites for housing development from steep hillsides, is significant but irresponsibly ignored all too often because there are not enough people with the appropriate professional skills in a position to influence early plans of those engaged in the building process.

2.5.3 Flooding (Plate Movement)

Flooding can also occur due to changes in topography following major earthquakes. Following the 26 December 2004 and 28 March 2005 earthquakes, the Sunda Plate has sunk by about 1m with respect to sea level. This has had a dramatic effect on towns such as Singkil (Figure 2b) and Rigaih, where large areas have been “lost to the sea” or highly susceptible to tidal flooding (the maximum tidal range along the Aceh coast is about 1.5m). As a result many villages have been displaced or have been made uninhabitable.

Where there has been significant loss of coastline due to large scale plate movements, one must consider the future viability of the affected settlements. Engineering solutions can be provided, but they will require detailed investigations and significant civil engineering works to provide a safe, flood free environment. Hydrological and topographical surveys will be needed to asses the validity of potential re-location sites, and re-location carefully planned to ensure access to utilities, community

facilities and livelihood activity. If only part of a community wishes to re-locate, consideration needs to be given to the on-going care and maintenance of the fragmented community which remains, as well as those who re-locate.

(a)   (b)

Figure 2 Examples of housing a risk due to non-tsunami hazards (a) landslides due to rainfall (b) inundation by the sea

3. HOUSING GUIDANCE AND LEGISLATION

3.1 Seismic Design Code

The Indonesian seismic design code (SNI.03-1726-2002) provides an appropriate methodology for designing against the forces induced by an earthquake. It is comparable to seismic design codes from USA, Japan and Europe. The intent of the code is to prevent damage in a small earthquake that has a high probability of occurring during the life of the structure (maybe several times), and to protect loss of life in a major earthquake that has a low probability of occurring during the life of the structure. In the later case the building may be significantly damaged but should not collapse. Unfortunately the design of single storey residential houses and other similar structures falls outside the scope of the Indonesian seismic code.

3.2 Building Regulations

In July 2005 the Ministry of Public Works issued a Building Code for Aceh. This document provides minimum requirements for the design of single storey residential houses termed "dwelling houses". Section 2 of the document provides the technical requirements for reliability of a building structure. These cover several design issues and principles which should be followed, including: building type and form, type and minimum dimensions of foundations, minimum column and beam dimensions, minimum reinforcement quantities and spacing, requirements for diagonal bracing and types of concrete mixes permissible.

During our first visit it became clear that the requirements of the Building Code were not being enforced, and many houses built at that time did not comply with these basic requirements (see Figure 3). Furthermore, it is noted that most international codes have restrictions on the use of unreinforced masonry for regions of moderate and high seismicity, such as Aceh. However, the Building Code for Aceh permits the use of masonry for walls panels, but provides no guidance on fundamental seismic principles including: maximum size of wall panels, openings in wall panels, minimum thickness of wall panel, tying of wall panels and provision of ring beams.

4. HOUSING IN ACEH

4.1 Housing Types

Housing in Aceh can be classified into three main categories, namely:

- The "permanent" houses, which are built from brick, often with reinforced concrete frames.
- The "semi-permanent" houses, which are built from brick and timber.
- The "traditional" houses, which are timber structures.

It should be noted that the definition of "permanent" and "semi-permanent" reflects terminology used during colonial times when the Acehnese were discouraged from building "permanent" houses in order to prevent acquisition of land title. "Semi-permanent" houses are therefore considered inferior.

Examples of these housing types are given in Figure 3. Most houses are the minimum size 36m2 "core" house, but frequently have veranda and/or kitchen extensions which increase the size up to 48m2 which is sufficient for a five person family based on a minimum of 9m2 per person. Most people in Aceh lived in "permanent" houses prior to the tsunami, and many where larger than those being provided.

4.2 Assessment Methodology

During the initial field mission ten different housing projects were reviewed as a benchmark of housing quality. This was done using a modified FEMA 154 approach (FEMA, 2002). Since, at that time, many of the houses were under construction, it was not possible to assess quality in terms of habitability, durability, access to water and sanitation, electricity and adequate communal facilities. The focus of benchmarking was therefore whether, both in terms of design and construction quality, the new houses were earthquake tolerant. During the second mission the other issues were also be assessed.

"Permanent" "Semi-permanent" "Traditional"

Figure 3 Examples of housing types

4.3 Key Observations

The key observations from the initial field surveys were as follows:

- "Permanent", "semi-permanent" and "traditional" timber houses have been constructed, though most of the "semi-permanent" houses were intended as transitional shelters only.
- The design and workmanship quality for many houses (reinforced concrete frame with unreinforced masonry infill) were found to be very poor when reviewed using the FEMA 154 approach. Many new constructions are thought likely to collapse in the next major earthquake.
- It was interesting to note however that the good examples were designed by experienced engineers and used a high degree of on-site supervision to assure that the quality of construction met the design intent.
- A variety of other construction methodologies including pre-cast frames, and reinforced blockwork has been used for "permanent" houses. These structural systems have all been developed by experienced engineers, to withstand earthquakes.
- The lightweight construction of "traditional" housing means these houses will probably meet life safety criteria, and their seismic resistance depends less on either design or workmanship. However, there was evidence of other problems including leaks due to poor workmanship or timber shrinkage, and termites.

As a consequence of our observations Arup highlighted these issues to the agencies involved and provided general guidance to the rebuilding process (see http://www.arup.com/geotechnics/project.cfm?pageid=8403).

The key conclusions were:

- Experienced earthquake engineers should survey structures that survived the earthquake of 26 December 2004 and address the issue of retrofitting.
- Experienced engineers should develop a basic and comprehensive code of practice for post-tsunami housing, and possibly a complimentary training programme to reinforce it.

- Procedures should also be developed to regulate the quality of construction. These are critical to deliver a product that is fit for purpose, and reduce vulnerability to future events. In particular experienced engineers should review construction of critical facilities; hospitals, schools, bridges etc.
- An education programme on hazards should be implemented at all levels of government, in NGOs, and within the wider community to raise awareness.

Openings/Wall Panels

Concrete Quality

Quality of Materials

Figure 3 Examples of poor workmanship

This was just one of several initiatives during 2006 to address these concerns. On the second mission we were very pleased to observe a marked improvement in the quality of both design and workmanship of the housing. Many agencies had employed experienced engineers and/or contractors to achieve these improvements. Furthermore there was often a large degree of training to develop a more skilled local workforce. However, some construction issues still remain.

The second mission also allowed the issues of habitability, durability, access to water and sanitation, electricity and adequate communal facilities. A series of questionnaires were developed to understand whether these issues had been properly addressed. It became apparent that many agencies had taken a holistic approach, which encompasses these factors, so that the houses that they were building could become homes that families could live in and grow. Furthermore, based on local government statistics, it was clear that the occupation rates for those agencies who had just delivered houses were much less than those who had taken the holistic approach.

5. SITE SELECTION

Site provision was the responsibility of the local Government. There appeared however, to be no formal process, either within local government or the various agencies, for assessing the suitability of a site identified for development or carrying out the enabling and infrastructure works that may be required to ensure the selected site is viable. Typical site selection checklist, guidelines and background information can be found in Corsellis and Vitale (2005), Coburn et al (1995) and The Sphere Standards (2004).

There are many issues than can affect the site selection process, and they may be geographical, economic or political. One example where this has impacted is in the development of the US Aid Road from Banda Aceh to Calang. Many new houses have been demolished soon after their completion to make way for the new road.

Prior to commencing any housing program it is essential that the roles and responsibilities of various stakeholders are clarified. A site assessment should be carried out at each location to identify the needs for local infrastructure, identify who is responsible for implementation, and how this impacts on the housing programme. It is also recognised that short term and long term solutions for water supply may be required. It is also noted that water supply was a large problem in Aceh prior to the tsunami.

6. CONCLUSIONS AND PRACTICAL RECOMMENDATIONS

This paper summarises the findings of the authors following two missions to Aceh in early 2006 and late 2007. It is hoped that the principal findings can help direct further work in Aceh and influence the decision making process carried out in other post-disaster situations and where disaster risk reduction is being implemented.

- There a number of different natural hazards that should be considered in providing new housing for those affected by the tsunami.
- The consequences of volcanoes and large tsunamis are impractical, if not impossible to design against, and can only be mitigated through management, education and planning. This includes early warning systems, evacuation plans and routes which should be accounted for in urban planning and site layouts.
- Risks including flooding, landslides, and fault rupture can be avoided completely by locating houses away from these hazards. However, this is not always possible, particularly where people wish to re-build on their own land which is at risk. Alternatively these risks can be mitigated to some extent by providing well engineered drainage systems, and earthworks. The need, cost and timescale for carrying out such works, must be considered at the outset as part of a site selection process.
- The post conflict and disaster situation place severe stress on traumatised communities and requires careful managements to ensure appropriate quality and speedy delivery of housing whilst also resolving land rights issues to avoid future problems.
- Providing appropriate training to those who actually do the construction will ensure that the construction workforce has a greater understanding of seismic design considerations, the special

significance of good quality robust seismic detailing to ensure houses will withstand future earthquakes safely, and their vital role in ensuring that houses are compliant with the appropriate requirements.

- The importance of specifying the appropriate quality for the raw ingredient that are used to build
- The importance of high quality and functional detailing to ensure correct construction.
- The importance of quality control and quality assessment, especially in a post disaster or conflict environment.

In the end however, the most important issue is that we recognise the needs of the people who have been affected by these and similar tragedies. An earthquake tolerant house is an engineer's goal, but we must also recognise the people's needs and follow a holistic approach in the construction process. The new houses therefore need adequate water and sanitation, access to community facilities, electricity etc., and only then will these houses became homes where families and communities can re-build their shattered lives.

REFERENCES

Coburn, A., Hughes, R., Pomonis, A. Spence, R (1995), Technical Principles of Building for Safety. Intermediate Technology Publications.

Corsellis, T. and Vitale, A. (2005) Transitional settlement displaced populations. University of Cambridge Shelter Project, Oxfam.

FEMA (2002) Rapid Visual Screening of Buildings for Potential Seismic Hazards: A Handbook, FEMA 154, 2nd Edition

McCloskey, J., Nalbant, S.S. & Steacy, S. (2005). Earthquake risk from co-seismic stress. *Nature*. **434**, 17 March 2005, 291.

Nalbant, S.S., Steacy, S., Sieh, K., Natawidjaja, D. & McCloskey, J. (2005). Earthquake risk on the Sunda trench. *Nature*. **435**, 9 June 2005, 756-757.

Sieh, K. (2005). What happened and what's next. *Nature*, **434**, 31 March 2005, pp573-574.

The Sphere Project (2004) Humanitarian Charter and Minimum Standards in Disaster Response.

TSUNAMI WAVE PROPAGATION ALONG WAVEGUIDES

Andrei G. Marchuk

Institute of Computational Mathematics and Mathematical Geophysics
Siberian Division Russian Academy of Sciences, 630090, Novosibirsk, RUSSIA
mag@omzg.sscc.ru

ABSTRACT

This is a study of tsunami wave propagation along the waveguide on a bottom ridge with flat sloping sides, using the wave rays method. During propagation along such waveguide the single tsunami wave transforms into a wave train. The expression for the guiding velocities of the fastest and slowest signals is defined. The tsunami wave behavior above the ocean bottom ridges, which have various model profiles, is investigated numerically with the help of finite difference method. Results of numerical experiments show that the highest waves are detected above a ridge with flat sloping sides. Examples of tsunami propagation along bottom ridges of the Pacific Ocean are presented.

Science of Tsunami Hazards, Vol. 28, No. 5, page 283 (2009)

INTRODUCTION

The qualitative theory of waveguides in a media with varying optical density (velocity of signals or waves in it) as well as the concept of waveguides with total reflecting boundaries have been discussed in the literature (Brekhovskikh [1]). Based on such previous work, the present study introduces the concept of waveguides in an application related to the tsunami problem. In a two-dimensional space the velocity of wave disturbance propagation caused by a sudden disturbance is constant and represented by $\mathbf{v}_0$. In a linear regime it decreases monotonically and reaches a minimum value along the axis. This linear axis where wave propagation velocity is less than $\mathbf{v}_0$ is named "waveguide". If a wave origin source is initially located on such waveguide, a portion of the energy will be captured and the waves will propagate along its length for a long time - more than likely to the very end of it. The present study examines the linearly varying but increasing wave propagation velocity along the axis of the waveguide. The postulated waveguides look like bottom ridges with flat sloping sides. A plane wave on the mean water surface is assumed to be the origin source and the initial propagation direction of the wave's front is along the waveguide's axis. The present study develops the quantitative theory of the wave propagating process for waveguides of this type.

Determination of wave rays above the sloping bottom.

Wave rays, widely used in wave kinematic investigations, can be determined as curves, orthogonally directing the propagating wave front at every moment of time. In other words they are the trajectories of wave front-line points during wave propagation. In an area of constant depth all such rays have the form of straight lines. Based on long-wave theory the propagation velocity for tsunami waves depends only on water depth and is defined by Lagrange's formula

$$c = \sqrt{gH} \,. \qquad (1)$$

Wave-rays can be defined as the quickest routes of a perturbation's propagation. Wave rays are the orthogonal lines of energy directivity along a tsunami's wave front. In ocean areas of variable depths, the wave rays do not usually follow straight line paths. Thus, in general, the problem of tsunami travel-time determination from one point to another, cannot be easily and accurately determined. The integral which describes the time required for a perturbation (tsunami wave) to move between points **A** and **C**, in the XOY plane is given by:

$$T = \int_{\gamma} \frac{dS}{c(x,y)}, \qquad (2)$$

where dS is an element of the γ curve, connecting the points **A** and **C** (Fig. 1).

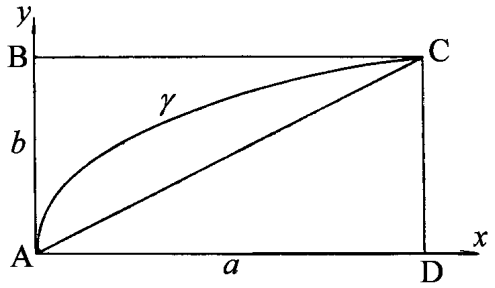

Fig. 1. Diagram of problem of determining the tsunami travel-time from the source to the point on the shore line (the wave-ray definition problem)

We must now determine the curve **γ** which minimizes the integral (2). After the trace determination it is easy to calculate the required tsunami travel-time from point **A** to point **C**. One of the possible ways in determining a wave front's ray trace is by numerical solution of the Cauchy problem and the use of governing differential equations. In the case of simple distribution of water depth *H(x, y)* one can find analytically the *y(x)* curve of interest, and obtain the explicit formula for the time required for tsunami wave propagation. We can also proceed with this procedure for a sloping ocean floor. The derived solution can explain some of the effects which take place during the tsunami wave propagation in the near shore zone.

Let us now consider the following problem: we have a rectangular section **ABCD** of the ocean, near the shore (Fig. 1). The sides are a and b long. The point **A**, which is on the shore-line, we shall assume to be the zero point of the Descartes coordinate system *XOY*. Let us also assume that the depth will increase linearly from **AD** side towards **BC** side, as per the following rule

$$H(x,y) = tg(\alpha)\cdot y\,,\ H(B) = H(C) = a\cdot tg(\alpha) = H_0\,,\qquad H(A) = H(D) = 0\,, \tag{3}$$

where α is the bottom inclination angle with respect to the horizon.

Let us also assume that at the point **C** at the moment in time $t=0$, a tsunamigenic earthquake took place. The problem is to determine the time interval at which the wave will reach point **A**. The earthquake generated tsunami wave will propagate in all directions but there is a certain optimal trajectory **γ,** along which the perturbation will reach point **A** at the shortest time. This is precisely the trajectory which we determine in order to find the time required for the propagation of this tsunami wave along this trajectory. As already stated, because of the relationship between frontal wave propagation rate and depth (1), the optimal trajectory is not a straight line, connecting **C** and **A** points. In fact, it will be a curve, which lies to the right of the AC diagonal line, in moving from the point C to the point A - in other words, in the area of greater depth (see Figure 1). Thus, the time of the wave movement along the y curve is given by:

$$T = \int_\gamma \frac{d\gamma}{\sqrt{gH}} = \int_\gamma \frac{\sqrt{dx^2+dy^2}}{\sqrt{g\cdot y\cdot tg(\alpha)}} = \int_\gamma \frac{\sqrt{1+(y')^2}}{\sqrt{g\cdot y\cdot tg(\alpha)}}dx = \frac{1}{\sqrt{g\cdot tg(\alpha)}}\int_\gamma \frac{\sqrt{1+(y')^2}}{\sqrt{y}}dx\,, \tag{4}$$

where $y' = dy/dx$. To solve the tsunami travel-time minimization problem it is necessary to determine the minimum of the integral (4) along all possible curves *y(x)***,** connecting the points **C** and **A**.

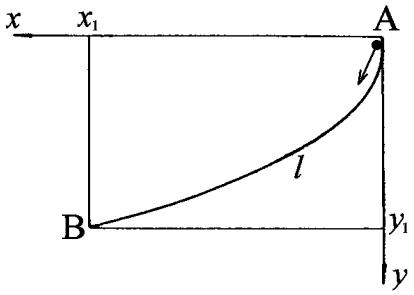

Fig. 2. Diagram of the brachistochrone problem

Let us now make use of the mechanical analogy, assuming that there are two points **A(0,0)** and **B(a,b)** located on the vertical plane *XOY*. In this case, the *OY* axis is directed downward and coincides with the force of gravity (Figure 2).

It is necessary to find such curve, connecting points **A** and **B**, along which a heavy ball, by rolling down under the force of gravity, from point **A**, will reach point **B** in the shortest time. Such ball starts its movement from a state of rest (brachistochrone problem). Because of the energy conservation law, the ball modulus of velocity can be expressed by the following formula:

$$v = \sqrt{2gy}\,. \qquad (5)$$

It can be easily seen that in this case the time required for this ball to move along the curve *l*, connecting points **A** and **B**, may be expressed as follows:

$$T_1 = \int_l \frac{\sqrt{1+(y')^2}}{\sqrt{2gy}}dx = \frac{1}{\sqrt{2g}}\int_l \frac{\sqrt{1+(y')^2}}{\sqrt{y}}dx\,. \qquad (6)$$

By comparing formulas (4) and (6) one can easily see that the time T and T_1, differ in terms of a constant factor

$$T_1 = \sqrt{\frac{tg(\alpha)}{2}}T\,.$$

In other words, we are to minimize the same integral as in the case, related to the tsunami wave propagation. The problem of the rolling ball is a classical problem of mechanics, which is solved by using the variation calculus method (Elsgol'ts [2]). Let us now express the ball's travel time (6) from the point **A**(0,0) to point **B**(x_1,y_1) as a functional of the curve shape $y(x)$

$$F\big(y(x)\big) = T\big(y(x)\big) = \frac{1}{\sqrt{2g}}\int_0^{x_1}\frac{\sqrt{1+(y')^2}}{\sqrt{y}}dx\,,\ y(0)=0,\ y_1=(y(x_1)). \qquad (7)$$

The integrand of this functional does not explicitly contain the x coordinate. So, the condition of minimum of this functional [2] is expressed as

$$F - y'F_{y'} = C\,,$$

where C is a constant. For this particular case (a rolling ball)

$$\frac{\sqrt{1+(y')^2}}{\sqrt{y}} - \frac{(y')^2}{\sqrt{y(1+(y')^2)}} = C\,. \qquad (8)$$

After simplifying we have

$$\frac{1}{\sqrt{y(1+(y')^2)}} = C\,,$$

$$y(1+(y')^2) = \frac{1}{C^2} = C_1\,. \qquad (9)$$

After introducing a new parameter ***t,*** which is defined as $y' = \mathrm{ctg}(t)$, formula (9) can be transformed to

$$y = \frac{C_1}{1+\mathrm{ctg}^2 t} = C_1 \sin^2 t = \frac{C_1}{2}(1-\cos(2t)),$$

$$dx = \frac{dy}{y'} = \frac{2C_1 \sin(t)\cos(t)dt}{\mathrm{ctg}(t)} = 2C_1 \sin^2(t)dt = C_1(1-\cos(2t))dt,$$

$$x = C_1\left(t - \frac{\sin(2t)}{2}\right) + C_2 = \frac{C_1}{2}\big(2t - \sin(2t)\big) + C_2.$$

Finally we have the parametric form of the curve, that provide the minimum of the ball's moving time

$$x - C_2 = \frac{C_1}{2}\big(2t - \sin(2t)\big),\ y = \frac{C_1}{2}\big(1-\cos(2t)\big),$$

Where $t=0$ at the starting point **A**(0,0). The constant C_2 is equal to zero, because the curve begins from the zero point **A**(0,0). After substitution $2t=t_1$ we will have equations of the cycloid (trajectory of the point on a circle during its rolling over horizontal line y=0) in parametric form:

$$x = \frac{C_1}{2}\big(t_1 - \sin(t_1)\big),\ \ y = \frac{C_1}{2}\big(1-\cos(t_1)\big),$$

where $C_1/2$ is the radius of the rolling circle, which can be determined on the basis of the cycloid passage through the point ***B***(x_1,y_1) (the second point is the starting point of the coordinates).
So, the solution of this problem, in other words, the optimal trajectory, would be a cycloid, which in its parametric form will be written as follows

$$x = C(t - \sin(t)),$$
$$y = C(1-\cos(t)). \qquad (10)$$

At the point (x_1,y_1), the t parameter value will be as follows

$$t = t^* = \arccos\left(1 - \frac{y_1}{C(x_1, y_1)}\right).$$

Further, the time of the movement of the ball, from the point A to point B along the cycloid may be expressed by the following integral:

$$\boldsymbol{T_1 = \int_0^{y_*} \frac{\sqrt{1+(y')^2}}{\sqrt{2gy}}dx = \frac{1}{\sqrt{2g}}\int_0^{t^*} \frac{\sqrt{1+\dfrac{\sin^2(t)}{(1-\cos(t))^2}}}{\sqrt{c_1(1-\cos(t))}}(1-\cos(t))dt =}$$

$$= \frac{1}{\sqrt{2g}}\int_0^{t^*}\sqrt{2C}\,dt = \frac{\sqrt{2C}}{\sqrt{2g}}t^*. \qquad (11)$$

Let's go back to the tsunami problem. If the tsunami wave propagates across the area with a sloping bottom, then instead of velocity $\sqrt{2gy}$ in formulas (6) and (11), there will be the value $\sqrt{g \cdot tg(\alpha) \cdot y}$. Consequently, for the tsunami travel-time between points *(a,b)* and *(0,0)* the following expression will be valid:

$$T = \frac{\sqrt{2C}}{\sqrt{g \cdot tg(\alpha)}} \cdot arccos(1 - \frac{b}{C}), \qquad (12)$$

where, as already mentioned, *C* is a constant, which is defined on the basis of the cycloid passage through the point *(a, b)*.

Investigation of waveguides using wave rays

Let us now study the process of tsunami wave propagation above the submerged ridge with flat sloping sides (Fig. 3). Let us also use the limited bottom slope with the fully reflecting boundary for such an investigation (Fig. 4). The 2D view on this rectangular water area with sloping bottom is presented in Figure 5. In the Cartesian coordinate system the depth is linearly increasing from zero on the **OX** axis ($y = 0$) by formula $H = y \cdot tg(\alpha)$, where α is inclination angle of the bottom slope.

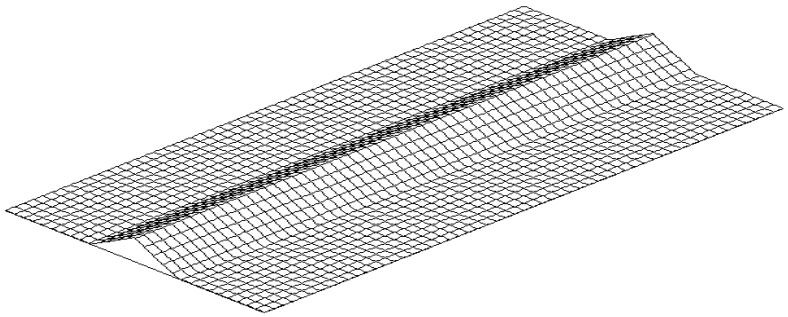

Fig. 3. A bottom relief simulating underwater mountain ridge

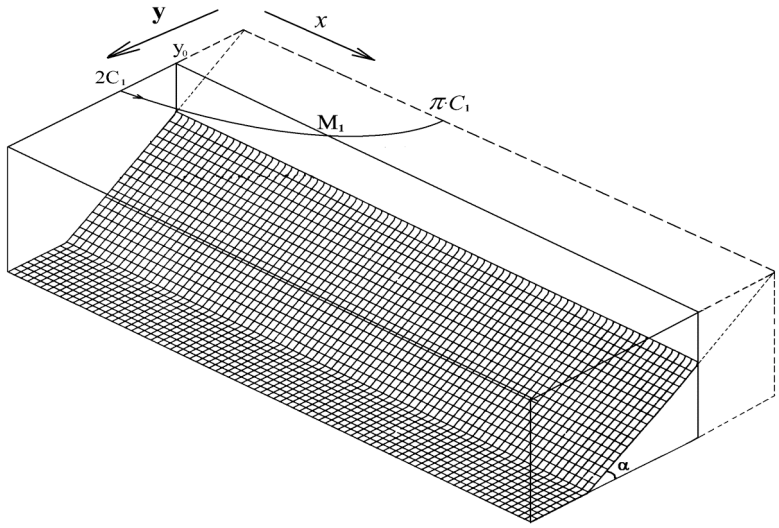

Fig. 4. 3D-view on a wave ray trajectory above the bottom slope

If from a point $(0, 2C_1)$ the wave ray started in parallel to OX axis direction, it will look like a segment of cycloid having radius C_1 (the radius of the rolling circle), and its trajectory can be described by equations

$$x = C_1(t - \sin(t) - \pi),$$
$$y = C_1(1 - \cos(t)), \quad t \in (\pi, 2\pi). \tag{13}$$

The ray will reach an axis OX in a point (x_2 , 0) (Fig. 5), where $x_2 = \pi \cdot C_1$. If the plane of bottom has the same declination, but the decreasing of depth stops on the line $y = y_0$ where the reflecting boundary is installed. The ray, after arriving to the point M_1 that is situated on the distance y_0 from the **OX** axis, will reflect from the line $y = y_0$. After reflection the wave ray will go to the point M_2 along the new cycloid with the same radius (see fig. 5). The condition of reflection of a wave ray on a line $y = y_0$, is caused by symmetry of a picture relatively to the axis $y = y_0$ that is true for symmetrical waveguides. The strip region $y_0<y<2C_1$ in Figure 5 simulates the sloping side of the bottom ridge (waveguide).

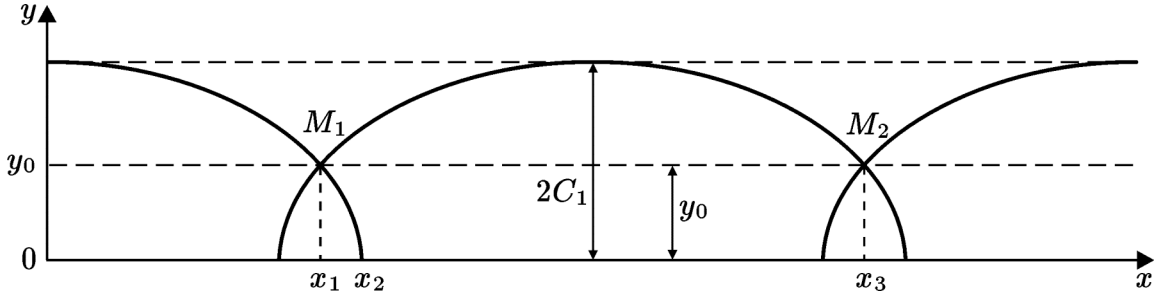

Fig. 5. Trajectory parameters during the wave ray motion above the bottom slope

Let us now determine the length of a step of this truncated cycloid, and also the wave travel time along it. As length of a step of a full cycloid is expressed as $L = 2\pi C_1$, the length of a step of a truncated cycloid (Fig. 5) will be expressed as follows

$$L_1 = x_3 - x_1 = L - 2(x_2 - x_1). \tag{14}$$

The value $(x_2 - x_1)$ easily can be define from the equation of a cycloid (13)

$$L_1 = 2\pi C_1 - 2C_1\left(\arccos(1 - \frac{y_0}{C_1}) - \sin\left(\arccos(1 - \frac{y_0}{C_1})\right)\right). \tag{15}$$

The wave travel-time along this cycloid can be written as follows

$$T = \frac{2\sqrt{2C_1}}{\sqrt{g \cdot \mathrm{tg}(\alpha)}}\left(\pi - \arccos(1 - \frac{y_0}{C_1})\right). \tag{16}$$

Here α is the inclination angle of the bottom plane to horizon, C_1 - radius of a cycloid. If maximum depth H_0 outside of the waveguide and minimum depth on a ridge H_1 is given, then

$$C_1 = \frac{H_0}{2\mathrm{tg}(\alpha)},\ y_0 = \frac{H_1}{\mathrm{tg}(\alpha)},\ l = (2C_1 - y_0), \qquad (17)$$

where l is a half-width of the waveguide, if the waveguide is twice wider (l_1=2l), but the depth variation remains the same. In this case the declination of bottom $\mathrm{tg}(\beta)$ will be reduced down to half of the former value and will become

$$\mathrm{tg}(\beta) = \frac{\mathrm{tg}(\alpha)}{2}.$$

Due to this, the radius of cycloid appropriate to "lateral" rays, reaching the edges (borders) of the waveguide, will be doubled, $C_2 = 2C_1$. The value y_2 also will increase ($y_2 = 2y_0$). The wave travel-time from the axis up to the edges of the waveguide along the new cycloid will be written as

$$T_2 = \frac{2\sqrt{4C_1}}{\sqrt{(g \cdot \mathrm{tg}(\alpha))/2}}\left(\pi - \arccos(1 - \frac{2y_0}{2C_1})\right) = 2T_1. \qquad (18)$$

The length of the cycloid step will be increased also by 2 times. Therefore, the average speed along the waveguide of the signals which propagate along "extreme" rays does not depend on the waveguide width and is determined only by the difference of depths H_0 and H_1.

Let us now investigate the propagation velocity of different segments of the wave front along the waveguide depending on their initial distance from the axis. In Fig. 6 the trajectories of the wave rays, which are started at distance $2y_1$ and y_1 away from the axis of the waveguide and the wave ray, traveling along the axis, are shown.

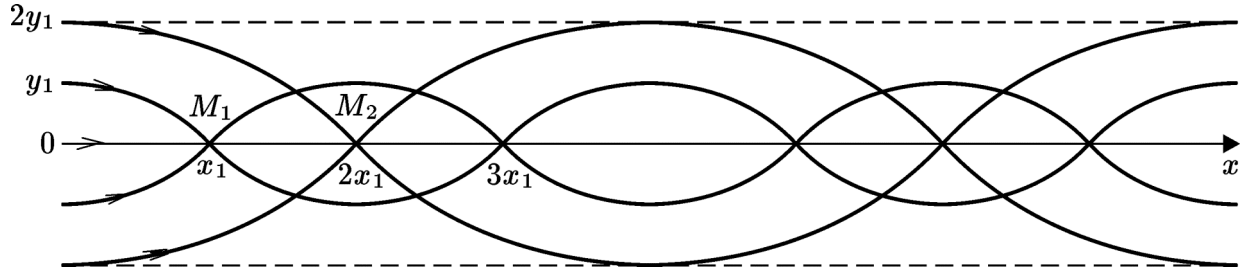

Fig. 6. Wave rays in the symmetric waveguide

Let l be the half-width of the waveguide, α - angle of inclination of the planes of bottom, H_0 - depth outside of the waveguide. The basic values we need for calculation are defined as

$$H_1 = H_0 - l \cdot \mathrm{tg}(\alpha),\ y_0 = H_1 / \mathrm{tg}(\alpha), \qquad (19)$$

where H_1 is the depth above a ridge. The value C_1 (radius of cycloid) depends on initial distance y_1 from an axis of the waveguide to a wave-ray starting point

$$C_1 = (y_0 + y_1)/2,\ \ 0 \le y_1 \le l.$$

Using expressions (15) and (16) the ratio between an average wave velocity V along the waveguide and value y_1 (or C_1) can be defined

$$V = \frac{L}{T} = \frac{2\pi C_1 - 2C_1\left(\arccos(1-\frac{y_0}{C_1}) - \sin\left(\arccos(1-\frac{y_0}{C_1})\right)\right)}{\frac{2\sqrt{2C_1}}{\sqrt{g\cdot tg(\alpha)}}\left(\pi - \arccos(1-\frac{y_0}{C_1})\right)}, \qquad (20)$$

where the values C_1 and y_0 are determined by formulas (17). The velocity of an appropriate wave motion along the waveguide depends on value C_1 (or y_1) and it is as less, as closer the initial wave ray to the axis. Let's find a speed limit V, when parameter y_1 is going to y_0. Let y_0 differs from y_1 by a small value ε.

$$y_0 = y_1(1-\frac{\varepsilon}{2}) = 2C_1 - \varepsilon C_1 .$$

Then, keeping in the formula (20) members of the least order by ε, we arrive at

$$V \approx \frac{2C_1\left(\pi - (\pi - \sqrt{\varepsilon}) + \sqrt{\varepsilon}\right)}{\frac{2\sqrt{2C_1}}{\sqrt{g\cdot tg(\alpha)}}\left(\pi - (\pi - \sqrt{\varepsilon})\right)} = \sqrt{2gC_1\cdot tg(\alpha)}, \qquad (21)$$

that corresponds to a disturbances propagation velocity along the axis of waveguide calculated by Lagrange formula $V = \sqrt{gH_1}$, which is applied to the top of ridge

$$C_1 = \frac{H_1}{2tg(\alpha)} .$$

Thus, each waveguide (not only with flat bottom planes) has a specific dispersion, which is discovered in expansion of the initial plane wave along the waveguide during its propagation. Finally the initial single wave will transform into a wave "train". This dispersion ability of each waveguide can be measured by value $q = V_{\max}/V_{\min}$, where V_{max} is the running speed of fastest rays along the waveguide and V_{min} the running speed of the slowest wave ray that coincides with the axis of waveguide.

Let us subsequently study the problem of wave energy focusing by the waveguide. Above a flat bottom the amplitude of a circle tsunami wave is decreasing due to cylindrical divergence proportionally $R^{-1/2}$, where R - distance from a source. Getting into the waveguide, the wave amplitude is not more decreased due to cylindrical divergence. However from this moment the wave energy disperses by stretching the initial single wave along the axis of waveguide, that also causing reduction of amplitude. If the rate of amplitude loss due to wave dispersion along the waveguide is less than the possible amplitude loss due to cylindrical stretching of the front, in this case a waveguide has focusing properties. Mathematically it can be written as follows:

$$(V_{\max} - V_{\min})\cdot T < \frac{2\pi}{K} R^{1/2} . \qquad (22)$$

Here T - time of motion of a waveguide waves, K - value indicating, what part of circle front of an incident wave has got in the waveguide, R - distance from the wave source up to a position of front in the waveguide after time period T. Thus, not every waveguide causes a focusing effect. It is the broader waveguides with small depths differences $(H_0 - H_1)$ that have the greatest focusing ability. The most favorable situation for focusing arises when the tsunami wave source is situated above the waveguide.

Let us now remark about asymmetrical waveguides, where the declination of flat bottom is various for different sides from the ridge. Let the declination of one side be 2 times greater, than the other. The depth outside the waveguide is equal to H_0 and on the ridge (axis) - H_1. Let us consider trajectories of "lateral" rays, which reach the borders of the waveguide. In the initial moment they lay out on distances y_2 and $y_1 = 2\,y_2$ on both sides from the axis of waveguide (Fig. 7).

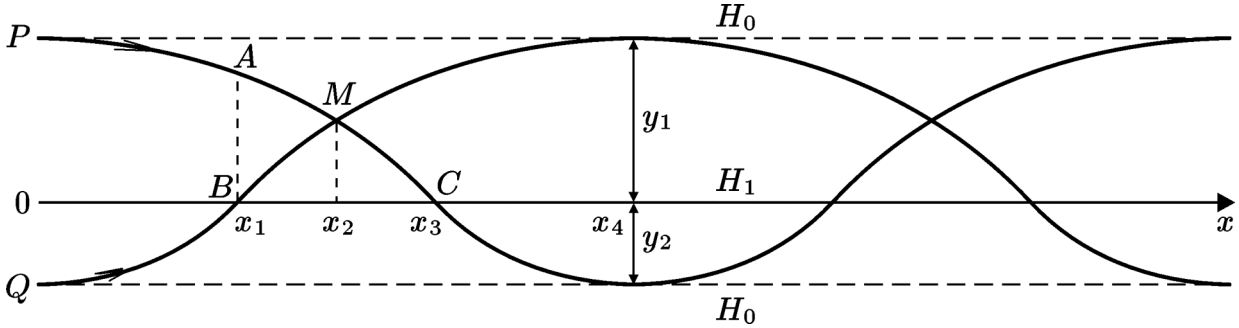

Fig. 7. Trajectories of "lateral" rays in an asymmetric waveguide

As previously-stated, the radius of cycloids, along which wave rays propagate above the more flat side, is twice greater than the radius of both of the rays under consideration, when propagating above the other side which has greater inclination. As seen in Figure 7, both rays have identical-length paths before reaching cross-section $x = x_4$, and each consisting of two cycloid pieces. Thus, on the cross-section $x = x_4$ the rays arrive simultaneously. The cross point **M** of these "lateral" wave rays is not located on the axis of the waveguide **Ox**. In spite of point **M** being a cross point of wave rays (a caustic), the noticeable increase of a wave amplitude in it is not detected, because the rays do not come to this point simultaneously. Let us show this as $y_1 = 2y_2$, then $x_3 = 2x_1$. The wave travel-time along the "large" cycloid is more than twice as that along the "small" (time $\mathbf{T_0}$). Taking into account that the travel-time along the curve **PC** is equal $2\mathbf{T_0}$, the travel-time along the curve **PA** will be less than $\mathbf{T_0}$, because the length of **PA** is less than the length of **AM**. Furthermore, along **PA** the depths are greater. Moreover, the wave travel-time along the curve **AM** will be less, than along **BM**, because the length of **AM** is less than the length of **BM**, and the curve **AM** is located along greater depth. Thus, the wave reaching point **M** along the curve **PM** will arrive much earlier, than that along the curve **QM**. Let us also estimate the propagating velocity of "lateral" rays along the waveguide, i.e. V_{max}. These rays will arrive simultaneously at the cross-section $x = x_4$ and their travel-time will be $3\mathbf{T_0}$. Therefore the average wave speed along the waveguide is expressed as x_1 / T_0, that is equal to V_{max} for symmetrical waveguides with the same depths on a ridge and the outside of the waveguide. Therefore the statement about the independence of the wave propagating velocity along the waveguide from its width is correct also for asymmetrical waveguides.

Now - as mentioned above - let us consider a ratio of tsunami amplitudes in the wave train that arises as a result of dispersion. Using relation (20), we find some values of propagating velocity **V** along the ridge for wave rays, which are disposed at different distances from the axis of

the waveguide. The derived values of propagating velocity **V** for that waveguide, suggest that the relation **V** from y_1 is rather close to linear, but for rays initially disposed closer to the waveguide edge, the varying rate of **V** depending on distance y_1 is lower than for rays initially located closer to the axis of the waveguide. Thus, the dispersion of the waveguide impacts a little bit stronger on the slowly moving part of a "wave train" and, consequently, the leading waves from a dispersing signal have slightly greater amplitude, than in the "tail" of the same "wave train".

In the case when on an entrance of the waveguide is perpendicular to its axis there are not one, but two consecutive waves. Let us assume that between positive maximums of these waves the initial distance is equal to 2λ. Then above the waveguide the waves will transform into "wave trains". The "leading" part of the second wave can reach the "tail" of the first wave and that will cause amplification of wave amplitude above an axis of the waveguide. It is possible to determine the causing conditions. Assuming that the initial distance between wave maximums in the waveguide is equal 2λ. Let the maximum and minimum wave rays propagating velocities of the waveguide be equal to V_{max} and V_{min}. The distance between the "tail" of the first wave and "leading" part of the second wave will be expressed as

$$l = V_{\min} \cdot T + 2\lambda - V_{\max} \cdot T, \qquad (23)$$

where T is the propagating time. Therefore, in time T_0, when l will become zero, the dispersed signals from both waves will be imposed on each other, and that will cause the amplification of oscillations near the axis of waveguide on the distance $T_0 \cdot V_{min}$ from its beginning. Hereinafter if there is imposing (superposition) of signal, the oscillation frequency in the waveguide fades out, as the process of waveguide dispersion promotes easing (attenuation) of both wave trains. Thus, the maximum level fluctuation in the waveguide is watched apart $T_0 \cdot V_{min}$ from a beginning of the waveguide. The time period T_0 is determined by the characteristics of the waveguide

$$T_0 = \frac{2\lambda}{V_{\max} - V_{\min}}. \qquad (24)$$

If the initial wave signals, propagating in the waveguide, have negative parts, then a picture of interaction of this waveguide waves will be more complicated.

Numerical experiments

To confirm the theoretical description of tsunami wave behavior in the waveguide of the indicated type, numerical modeling was carried out of tsunami wave propagation above underwater ridge, having a model relief as shown in Figure 3. A numerical algorithm based on variables splitting method (Titov [3]) was used for tsunami propagation modeling. The size of the computational area was 720 km x 400 km (720 x 400 grid-points), and the width of the waveguide was 200 km. The depth along an axis of the waveguide was equal to 500 m, and outside of the waveguide - 1,000 meters. The input tsunami was 4 meters high and was shaped as a long narrow rectangle (20 x 200 grid-points) with the profile, which is determined by the expression

$$\eta = 2 + 2\sin\left(\frac{i\pi}{10} - \frac{\pi}{2}\right), \text{ (i=1,...,20).} \qquad (25)$$

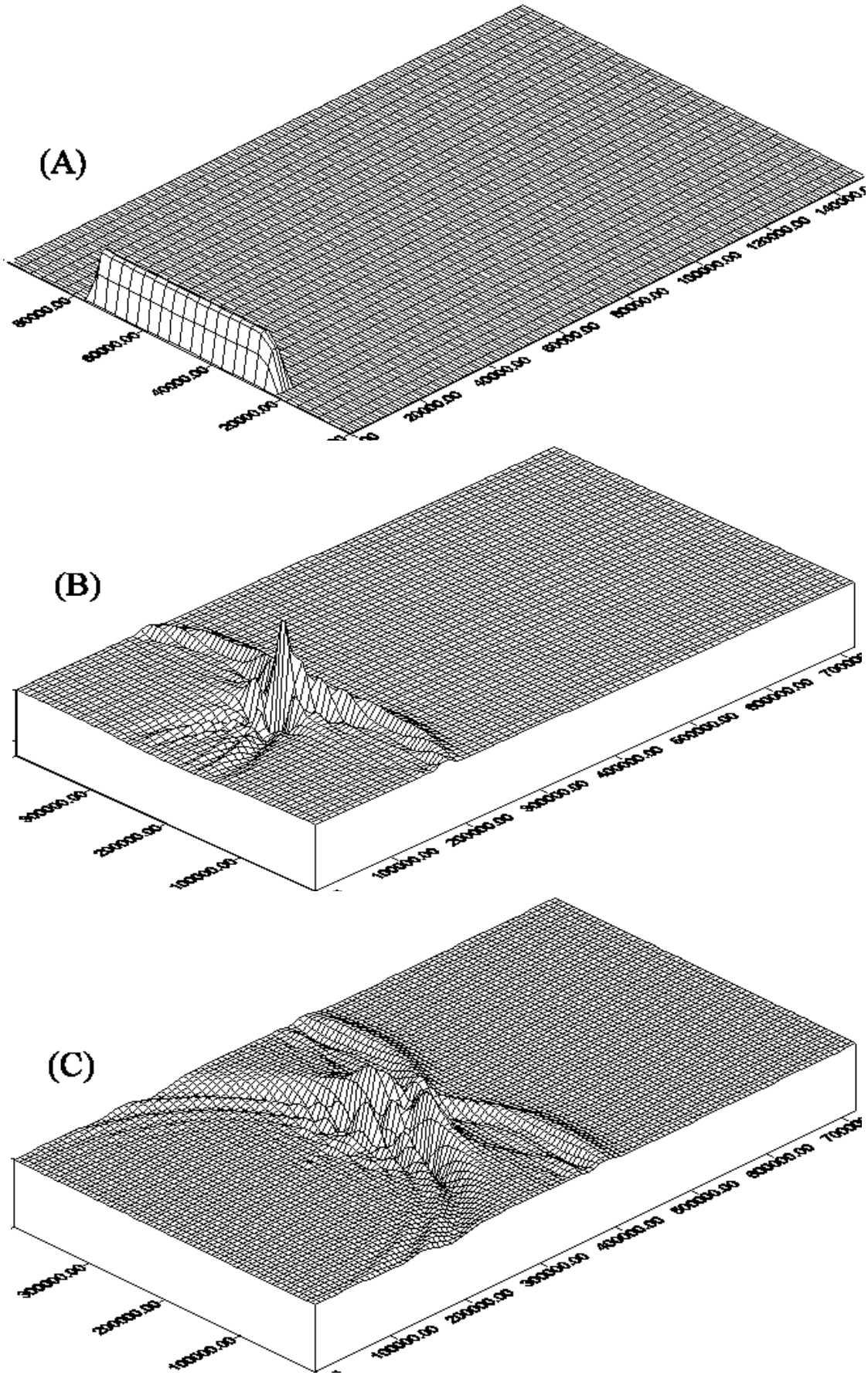
(A)
(B)
(C)

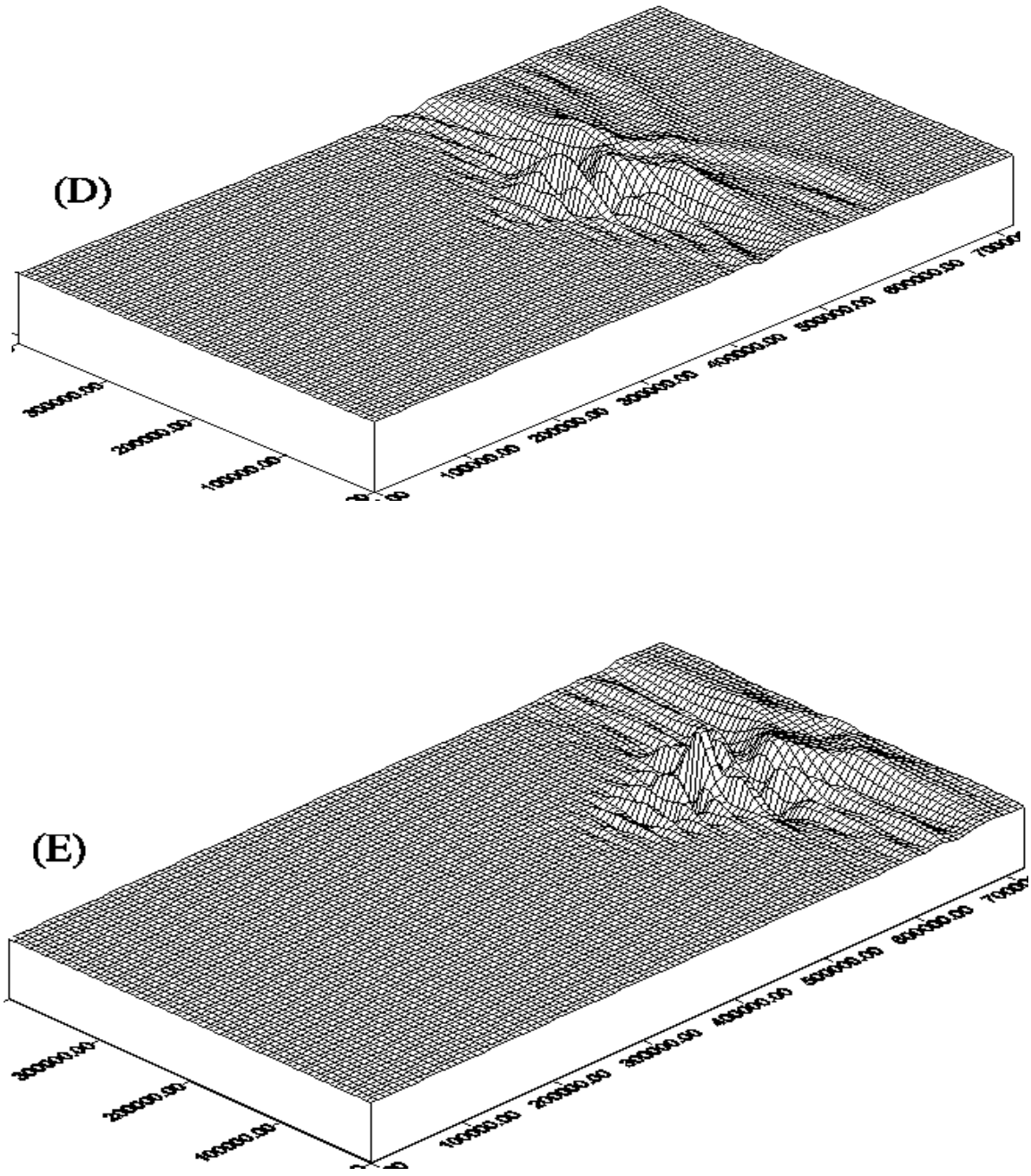

Fig 8A-8E. Water surface above the waveguide in various time moments

Figures 8A-8E show the ocean surface in different moments of wave propagation along the waveguide with flat sides (Fig. 3). The initial elevation of the water surface (fig. 8A) is forming a 2 meters high tsunami wave. The water surface at subsequent moments of time (2000 sec, 4000 sec, 8000 sec, 10000 sec) is shown in Fig. 8B-8E. As shown, that initial wave expands along the axis of waveguide and is transformed into a “wave train" with narrow front that completely confirms the theoretical results.

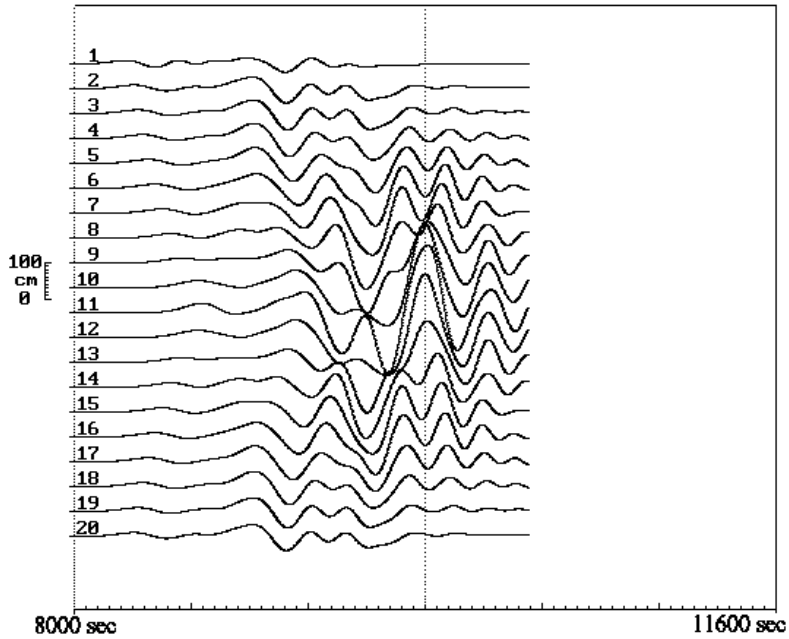

Fig. 9. Tsunami time series across the waveguide.

Figure 9 shows tsunami time series (marigrams) at a distance of 650 km from the tsunami source (the total length of the computational area being equal to 720 km). These marigrams correspond to 20 grid-points (650, 100+10(j-1)), which are located across of the computational area. Here j=1…20 is an index of time series (Fig. 9). Numerical results confirm the wave amplitude growth at the waveguide axis. Time series with index 11 (Fig. 9) was recorded just at the waveguide axis. The maximum tsunami wave height was detected here.

The profiles of water surface along the waveguide axis at the different time moments are shown in Figure 10. The Figure 11 presents free surface profiles along the same line (j=200) for the case of flat bottom (depth is equal to 1000 m) without any bottom ridge. In both computational experiments the initial 4 meters high source (25) generates the identical 2 meters high wave (top drawings in Figures 10 and 11).

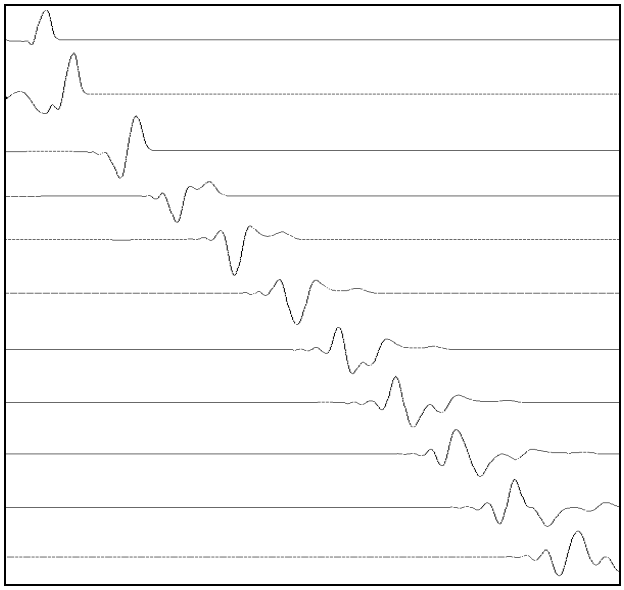
Fig. 10. Wave profile visualizations during tsunami propagation above the bottom ridge

As an example, let us estimate the average propagating velocities of fastest and slowest waves along this waveguide. For numerical computations the following parameters of the waveguide were used: H_0=1000 m, H_1=500 m. The fastest wave signal moves along the "lateral" wave ray having radius

$$C_1 = \frac{H_0}{2\mathrm{tg}(\alpha)} = \frac{y_1}{2},$$

where H_0 is the depth outside bottom ridge. The other parameters are linked by formula

$$y_0 = y_1/2 = C_1 .$$

Expression for the fastest wave propagation velocity (20) in this case will be written as

$$V = \frac{2C_1(\pi - \pi/2 + 1)}{\frac{2\sqrt{2C_1}(\pi - \pi/2)}{\sqrt{g \cdot tg(\alpha)}}} = \frac{\sqrt{2C_1 \cdot g \cdot tg(\alpha)}}{2}(1 + \frac{2}{\pi}) = V_0 \frac{(1 + 2/\pi)}{\sqrt{2}} \approx 1.17 \cdot V_0 .$$

Here $V_0 = \sqrt{gH_1} = \sqrt{gC_1 \cdot tg(\alpha)}$ is the slowest wave propagation speed (above the waveguide axis). This estimate is in good agreement with numerical results (Fig. 10).

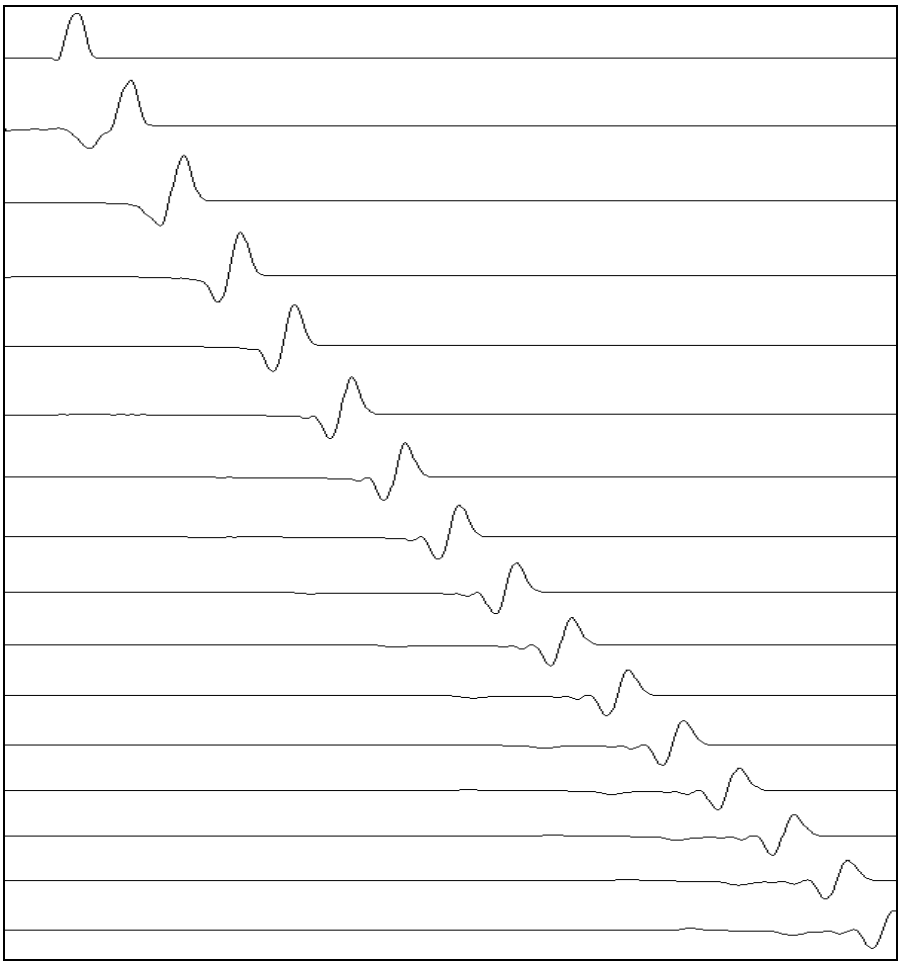

Fig. 11. Wave profile visualizations during tsunami propagation above the flat bottom

The comparison of wave amplitudes in the waveguide above the flat bottom indicates the significant amplitude growth above the axis (199 cm as compared to 85 cm without waveguide). In other words the amplitude of a tsunami wave which is propagating along this waveguide doesn't decrease during the first 3 hours of propagation.

A number of different ridge profiles were used in numerical computations. The profile of the bottom ridge was determined by the following formula

$$H(y) = H_1 + (H_0 - H_1)\frac{y}{y_0} - k \cdot \sin(\frac{\pi y}{y_0}), \qquad (26)$$

where y is the distance from an axis, H_1 - the water depth on the axis, H_0 - the depth outside the waveguide and **k** is parameter, which varies from -150 to +150. When k=0 the ridge sides are flat. Waveguide sections for k=-100, k=0, k=+50, k=+150 (from the top to the bottom of the figure) are shown in Fig. 12.

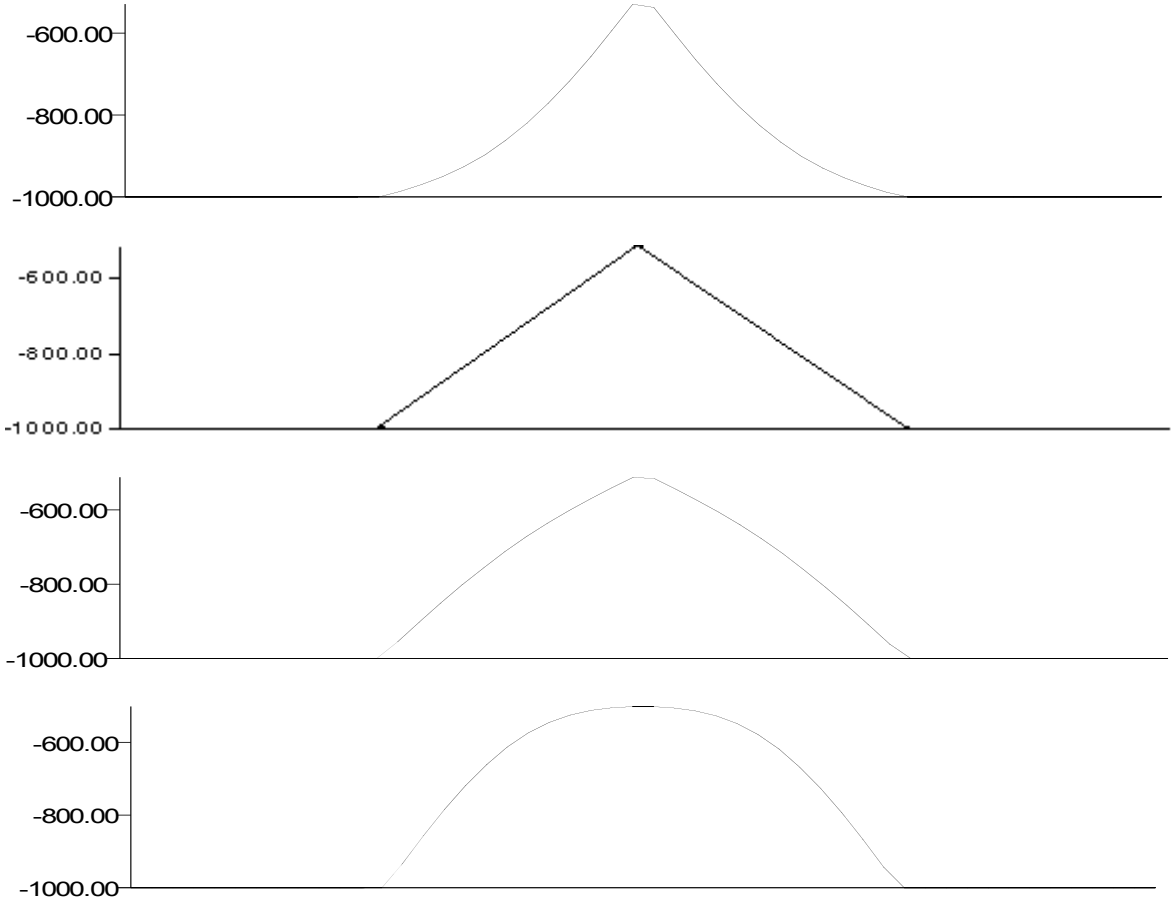

Fig 12. Profiles of the bottom ridge for different values of parameter **k**

The comparative analysis of numerical results presented in Table 1, leads to the conclusion that the most effective waveguide for the generated waves, is the one with flat sides (parameter k=0). Such a waveguide yields the greatest wave amplitude during propagation of a tsunami with the initial height of 2 meters (Table 1).

Table 1.

Coefficient ***k***	Minimum wave amplitude	Maximum wave amplitude
- 150	- 88	+ 87
- 100	- 82	+ 113
- 50	- 91	+ 121
0	- 167	+ 184
50	- 110	+ 119
100	- 73	+ 45
150	- 106	+ 60

Numerical modeling of tsunami propagation along the real Pacific waveguide was carried out with the model tsunami source, which produced the initial two meters high tsunami wave. The 600x720 points computational grid included the Izu-Nanpo island chain southward of Japan (Fig. 13). The bottom relief was taken from Smith-Sandwell 2 arc minute Global digital bathymetry [4]. The initial tsunami source has the same profile as in previous computation experiments but its length is equal to the whole computational area width (600 grid steps). Looking at Figures 14(a-c) it is seen that wave energy is concentrated above the bottom ridge. Tsunami waves here are much higher than ones outside this natural waveguide. The maximum of tsunami height was detected at the Izu peninsula, where the bottom ridge comes out from the deep ocean onto a shelf.

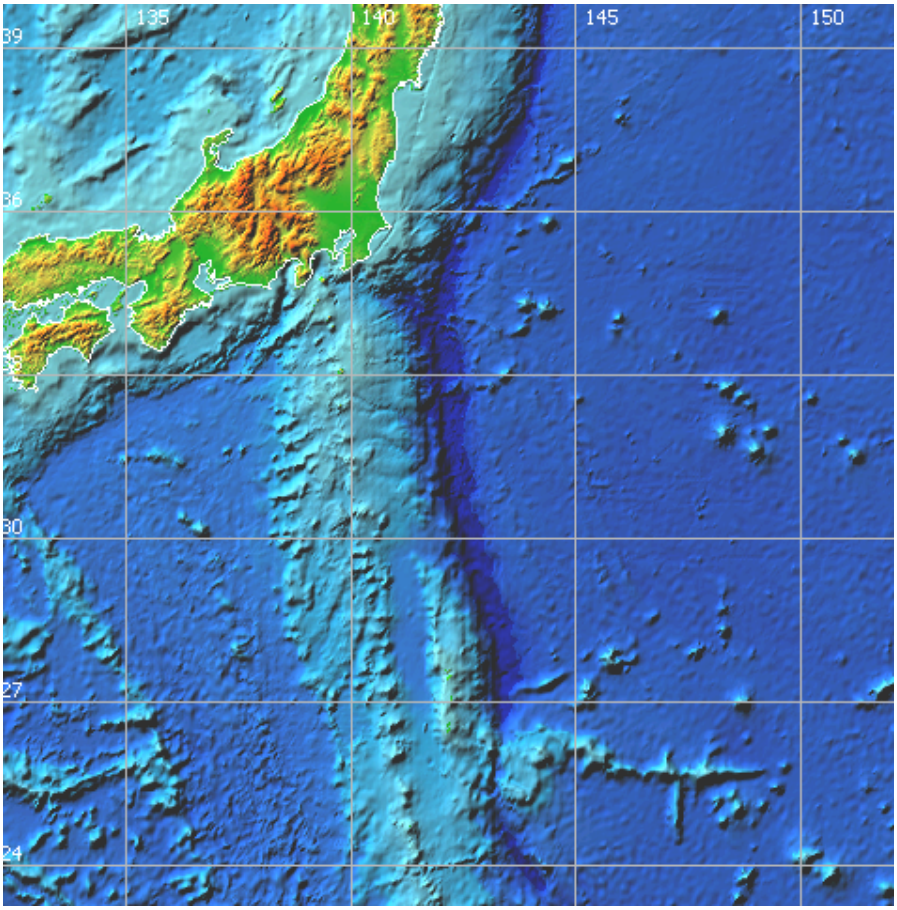

Fig. 13. The bottom relief in numerical computations of tsunami propagation along the Izu-Nanpo island chain

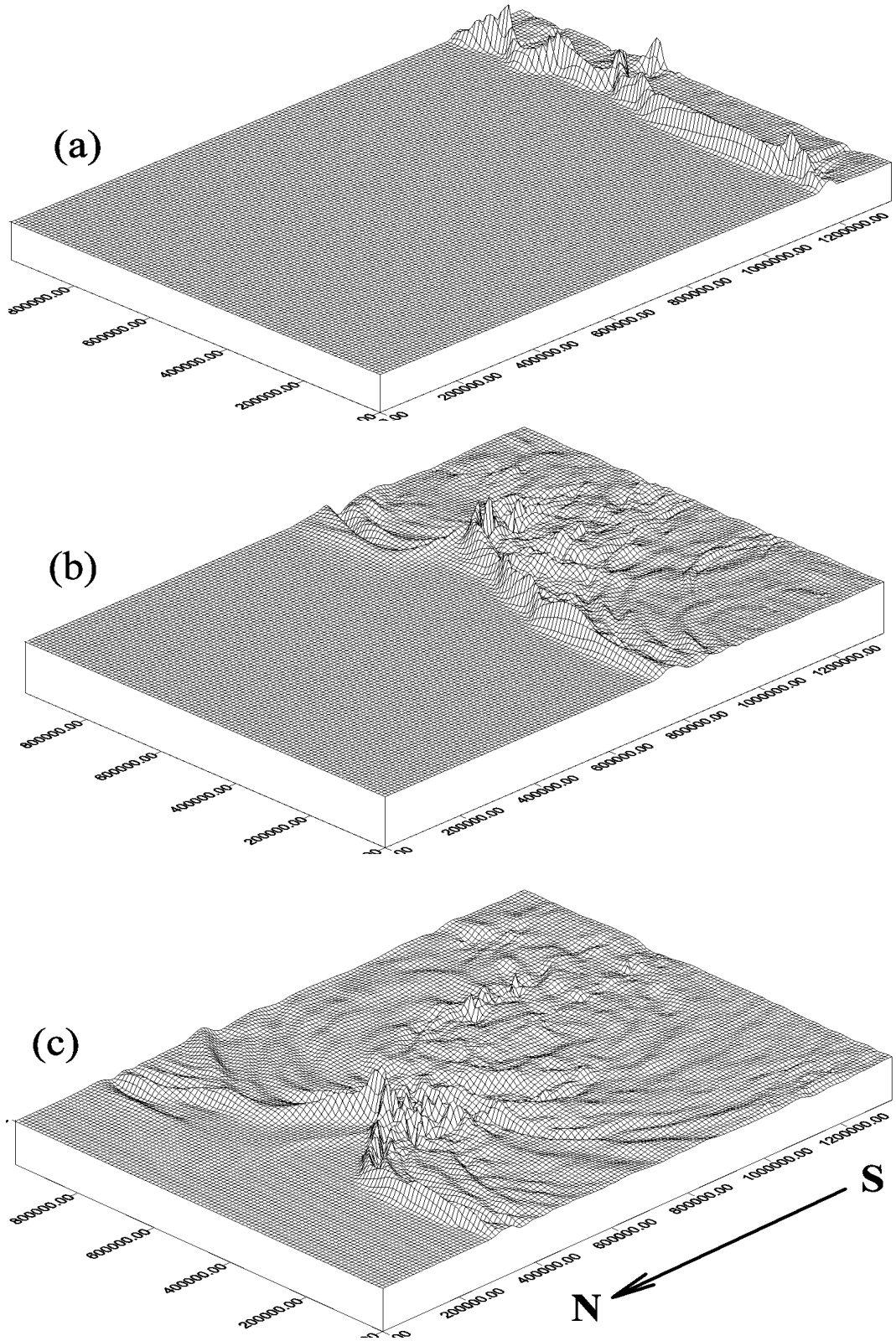

Fig. 14. Water surface during tsunami wave propagation above the Izu-Nanpo bottom ridge

Another example of the ocean bottom ridges influence to the tsunami propagation process can be found in another study [5]. In this paper some field data of tsunami 26 December 2004 and

results of numerical modeling of its global propagation are presented. Based on a comparative analysis of the maximum of the calculated amplitude in World Ocean (Fig. 15) and the World Ocean bathymetry (Fig. 16), it may be concluded that some bottom ridges (dash lines in Fig. 16) acted as tsunami waveguides. The travel-time charts of the tsunami of 26 December 2004 [5] also confirm the waveguide mode of tsunami propagation above some Pacific bottom ridges.

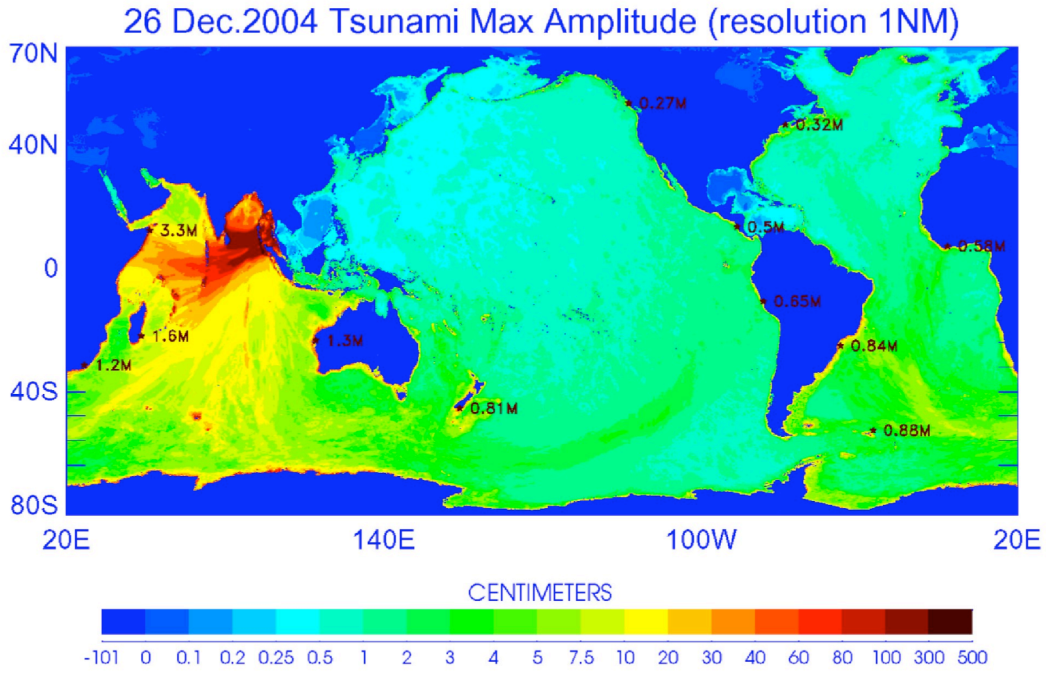

Fig. 15. Maximum of the calculated amplitude in World Ocean [5]

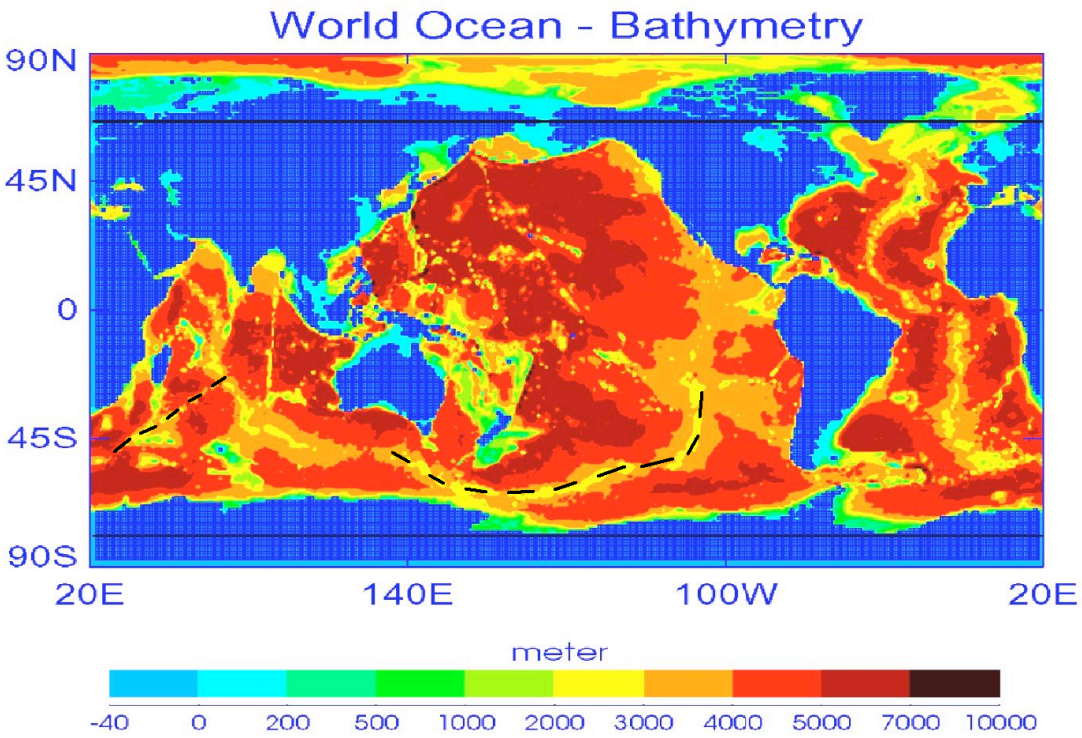

Fig. 16. Ocean bathymetry that was used for numerical modeling [5]

Acknowledgments

The work is supported by SBRAS Grant for Integration project No. 2006/113 and RFBR grants 07-05-13583, 08-07-00105.

References

1. Brekhovskikh, L.M., 1957, *Waves in stratified media* (in Russian) Moscow: USSR Academy of Sciences, 1957.
2. Elsgol'ts A.E., 1969, *Differential equations and a calculus of variations* (in Russian). Moscow, Nauka, 1969, 424p.
3. Titov, V.V., 1989, Numerical modeling of tsunami propagation by using variable grid. *Proceedings of the IUGG/IOC International Tsunami Symposium*, Computing center Siberian Division USSR Academy of Sciences, Novosibirsk, USSR, 1989, pp. 46-51.
4. Smith W.H.F. and Sandwell D. 1997. Global seafloor topography from satellite altimetry and ship depth soundings. *Science.* 277: 1956-1962.
5. Z. Kowalik, T. Logan, W. Knight and P. Whitmore, 2005. Numerical modeling of the global tsunami: Indonesian tsunami of 26 December 2004. *Science of Tsunami Hazards*, Vol. 23, No. 1, (2005), pp.40-56

TSUNAMI LOADING ON BUILDINGS WITH OPENINGS

P. Lukkunaprasit[1], A. Ruangrassamee[2] And N. Thanasisathit[3]

[1]Professor, Dept. of Civil Engineering, Chulalongkorn University, Bangkok, Thailand
[2]Assistant Professor, Dept. of Civil Engineering, Chulalongkorn University, Bangkok, Thailand
[3] Ph.D. Student, Dept. of Civil Engineering, Chulalongkorn University, Bangkok, Thailand

Email: lpanitan@chula.ac.th, fcearr@eng.chula.ac.th, nutwut@gmail.com

ABSTRACT

Reinforced concrete (RC) buildings with openings in the masonry infill panels have shown superior performance to those without openings in the devastating 2004 Indian Ocean Tsunami. Understanding the effect of openings and the resulting tsunami force is essential for an economical and safe design of vertical evacuation shelters against tsunamis. One-to-one hundred scale building models with square shape in plan were tested in a 40 m long hydraulic flume with 1 m x 1 m cross section. A mild slope of 0.5 degree representing the beach condition at Phuket, Thailand was simulated in the hydraulic laboratory. The model dimensions were 150 mm x 150 mm x 150 mm. Two opening configurations of the front and back walls were investigated, viz., 25% and 50% openings. Pressure sensors were placed on the faces of the model to measure the pressure distribution. A high frequency load cell was mounted at the base of the model to record the tsunami forces. A bi-linear pressure profile is proposed for determining the maximum tsunami force acting on solid square buildings. The influence of openings on the peak pressures on the front face of the model is found to be practically insignificant. For 25% and 50% opening models, the tsunami forces reduce by about 15% and 30% from the model without openings, respectively. The reduction in the tsunami force clearly demonstrates the benefit of openings in reducing the effect of tsunami on such buildings.

KEYWORDS: Tsunami loading, Building, Opening, Experiment, Pressure

1. INTRODUCTION

It has been observed that a large number of reinforced concrete (RC) buildings not designed for tsunami in Southern Thailand have survived the devastating 2004 Indian Ocean Tsunami. Furthermore, RC buildings with openings in the masonry infill panels have shown superior performance to those without openings (Lukkunaprasit and Ruangrassamee, 2008).

The tsunami loading on vertical walls has been experimentally investigated by Fukui et al. (1963), Cross (1967), Ramsden and Raichlen (1990), Ramsden (1996), and Hamzah et al. (2000). Cross also developed a simple theory to estimate the force exerted by a surge traveling over a dry bed and impinging on a vertical wall. Asakura et al. (2002) carried out two dimensional and three dimensional hydraulic model tests on a land structure behind a vertical seawall. Tsunami waves with various periods were generated in the investigation using both wave flumes and a wave basin, respectively. A practical formula was proposed for the wave pressure profile on the structure. Yeh (2007) reviewed existing design guidelines and proposed a rational methodology for determining tsunami forces on land structures using inundation map information.

Apparently there is little work on tsunami forces acting on 3-dimensional buildings, especially when openings are present. Thus, there is an urgent need to investigate tsunami loading on buildings with openings. The findings are useful for an economical and safe design of buildings, especially vertical evacuation shelters, against tsunamis.

2. EXPERIMENTS

A one - to - one hundred scale building model with square shape in plan was tested in a 40 m long hydraulic flume with a square cross section of 1 m x 1 m (Figure 1). A very mild slope of 0.5 degree, which represented the beach condition at Kamala, Phuket Thailand, was adopted for tsunami simulation in the hydraulic laboratory. The model dimensions were 150 mm x 150 mm x 150 mm. Three configurations of the front and back walls were investigated for wave forces, viz., 0%, 25% and 50% openings (Figure 2). Pressure sensors were placed on the front face of the model to measure the vertical pressure distribution. A high frequency load cell was mounted at the base of the model to record the tsunami forces. The tsunami wave was generated by a sudden release of water through a controlled gate at the bottom of the water tank located at the upstream end of the flume. Three nominal wave heights were investigated, viz. 40, 60 and 80 mm. The wave height is defined as the maximum inundation height that would occur in a flow without the presence of the model measured at the location of the model.

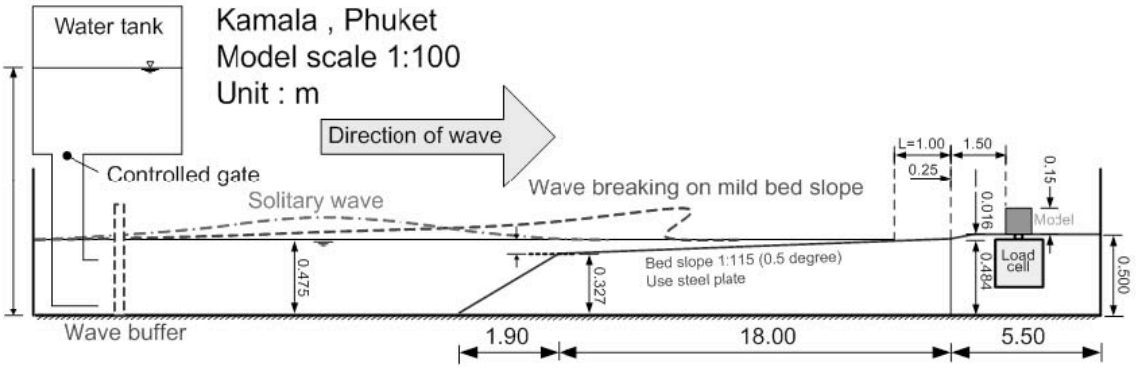

Figure 1 Experimental set-up

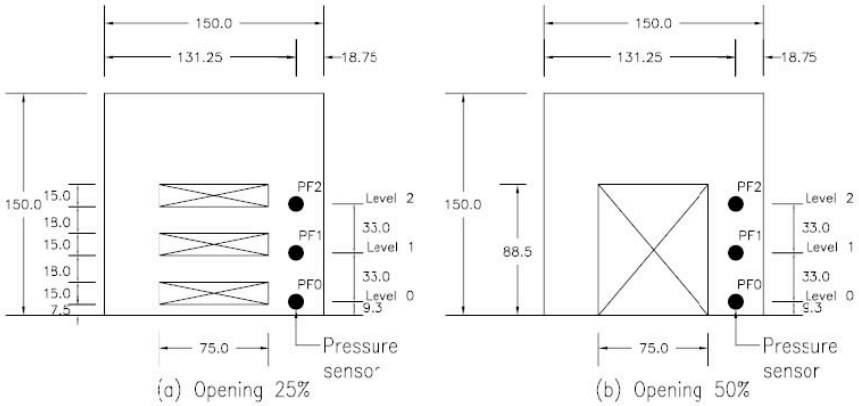

Figure 2 Configurations of the front and back panels of building model with sensor locations.

Figure 3 Formation of bore on slope beach (Nominal wave height = 80 mm)

3. Results

3.1. Velocity – Wave Height Relationship

The generated wave broke when approaching the beach at about 20 m upstream from the model, transforming into a bore before hitting the model (Figure 3). The typical time histories of the velocity of the wave and wave height at the location of the building model (in the absence of the model) are depicted in figure 4. It is to be noted that the leading edge of the wave attains a maximum velocity at the instant it reaches the location of interest when the wave height is still

very small. As the wave increases in height, the velocity decreases significantly. Figure 5 shows the relationship between the measured maximum velocity of the leading wave front, V, and the maximum wave height, h. The associated peak wave velocities generated varied from 2.4√(g*h) - 3.0√(g*h), where g is the acceleration due to gravity. In the absence of a laboratory test, it is not known in advance the value of V corresponding to a particular value of wave height. Thus, it is for convenience to express the maximum velocity in terms of the maximum wave height.

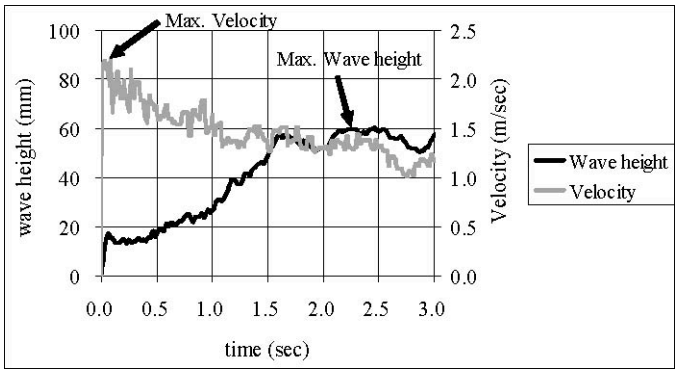

Figure 4 Typical time history records of wave height and velocity at location considered (without structure) - nominal wave height = 60 mm

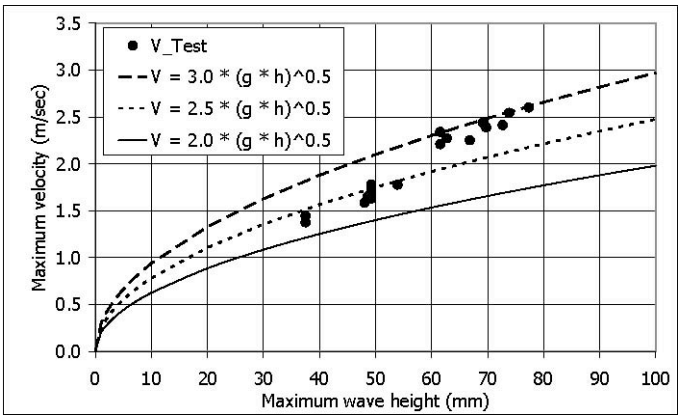

Figure 5 Relation between maximum velocity (V) and the maximum wave height (h)

3.2. Model Without Openings

When the leading edge of the wave hit the model, the wave splashed up its front face much like a wave striking a wall as depicted in the photo shown in figure 6. However, the energy imparted to the structure in the case of the 3-dimensional model was considerably less than that on a 2-dimensional wall (taller than the splash-up height) since part of the splash was diverted sideways upon impact, and part of it overtopped the model for the cases of 60 and 80 mm nominal wave heights with the splash reaching more than 2 times the model height. No overtopping occurred for the 40 mm wave height.

Figure 7 depicts typical time records of the pressures at the upstream face of the building model

without openings. As expected, one may note the high impact pressure at impingement of the leading tongue upon the model. Figure 8 shows the typical normalized pressure on the solid model (without openings) at different instants of time, corresponding to the attainment of peak pressure readings at different levels. The pressure distribution at the instant the wave force is maximum is also shown in the figure. It is noted that upon impingement of the leading tongue on the model, the pressure at the bottommost sensor (located at 9 mm above the base) attains a very high value of more than 4 times the hydrostatic pressure, and the pressure concentrates over approximately half the maximum wave height. As time progresses, the peak pressure near the base decreases while the values increase at higher levels. At the instant the wave force on the model is maximum, the peak pressure drops to about 2.4 times the hydrostatic pressure. The pressure profile associated with the maximum wave force can be conservatively approximated by a bi-linear distribution shown in Figure 8 with a value of 2.75 times the hydrostatic pressure over one wave height above the base and decreasing to zero at 2 times the inundation height. The pressure, p_i, at height z can thus be expressed as follows:

$$p_i / \rho g h = \begin{cases} 5.5 - 2.75\, z/h & \text{for } z/h > 1 \\ 2.75 & \text{for } z/h \le 1 \end{cases} \qquad (3.1)$$

where ρ is mass density of water.

It should be noted that designing the building using the pressure profile envelop would significantly overestimate the actual peak force exerting on the structure.

(a) front view (b) rear view

Figure 6 Snapshots of flow past the model at impact

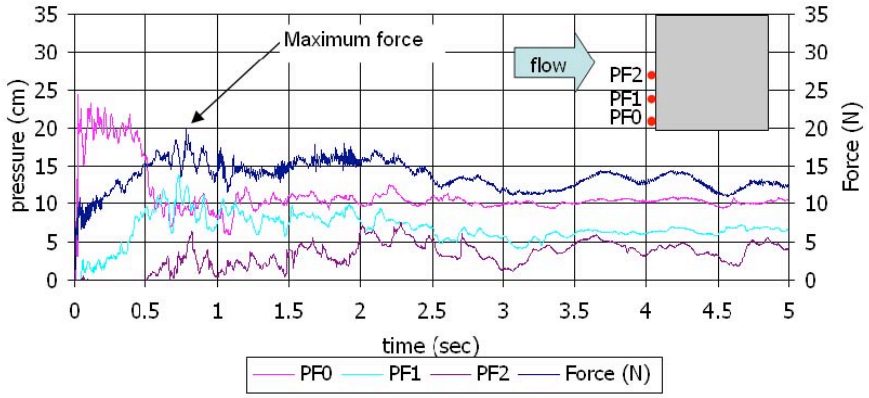

Figure 7 Typical time records of the pressures at the upstream face of the building model without openings

Figure 8 Typical normalized pressure at different instants of time at different levels (Nominal wave height = 80 mm)

The wave force-height curve computed based on the proposed pressure profile is practically the upper bound curve for the experimental results as depicted in the figure 9. Also shown in the figure are the hydrodynamic forces (drag forces) determined in accordance with FEMA 55 (2000) guidelines based on the maximum wave velocity measured from the experiments. It may be noted that the calculated drag forces on the model are, in general, larger than the experimental values by 12%- 44%.

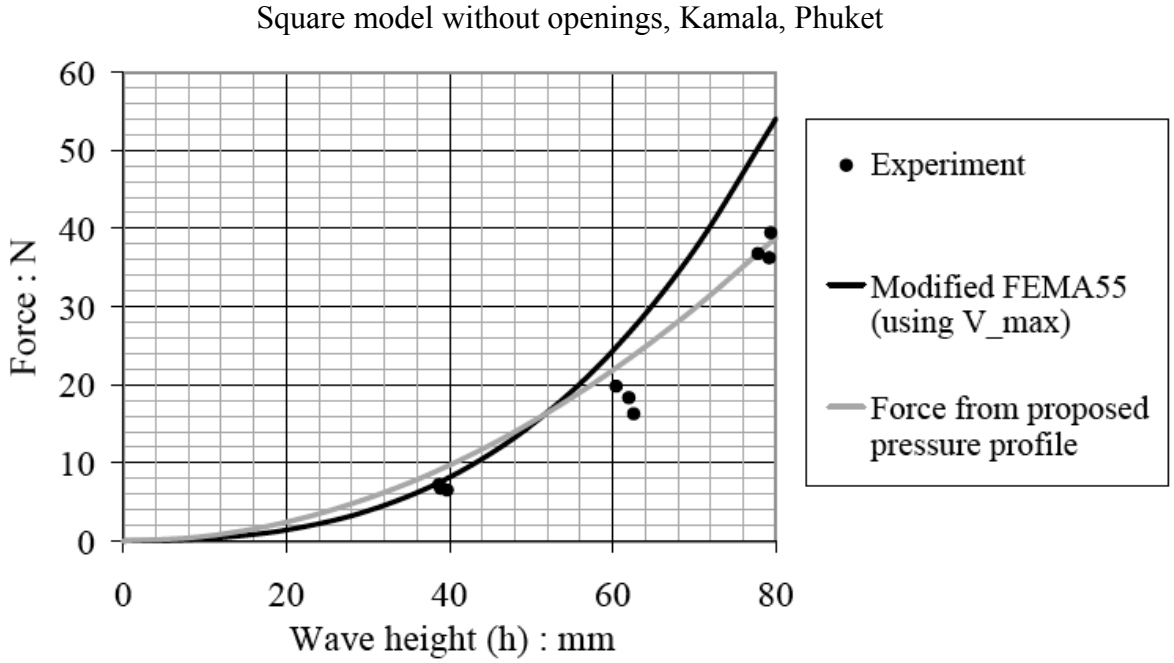

Figure 9 Comparison of tsunami forces obtained from experiments with those based on FEMA-55 guidelines

3.3. Effects of Openings

The influence of the openings on the peak pressures on the front panel of the model is found to be practically insignificant as can be seen in Table 1.

Table 1 Normalized pressure (Pi/ρgh) at positions PF0, PF1 and PF2 – square model with different openings

Opening	Nominal Wave height		
	40 mm	60 mm	80 mm
00%	6.8 (100%)	18.1 (100%)	37.9 (100%)
25%	5.1 (75%)	15.5 (85%)	31.5 (83%)
50%	4.3 (63%)	11.2 (62%)	26.2 (69%)

Note: PF0, PF1 and PF2 denote pressure sensor on the front face of model at levels 9.3 mm, 42.3 mm and 75.3 mm above the base, respectively.

Table 2 shows the variation of tsunami force, Fs, on the model with wave height for various opening configurations. It should be noted that Fs is the wave force acting on the whole structure and, for the case of models with openings, it includes the forces exerted by the wave on both the front and back panels of the model. Since the pressures on the upstream face of the model is not significantly affected by the presence of openings as discussed earlier, the reduction of the tsunami force on the upstream panel may be taken as proportional to the reduction in the panel area by the openings. Thus, for the case of 50% opening, in the absence of test results one may have to approximate the total force Fs to be equal to that acting on a solid model (without opening).

However, as evidenced in the test results in table 2, Fs decreases by about 30-40% in comparison with the solid model. The corresponding reduction is about 15-25% for the case of 25 % opening.

Table 2 Tsunami force (N) on square model with different opening configurations

Opening	Nominal Wave height								
	40 mm			60 mm			80 mm		
	PF0	PF1	PF2	PF0	PF1	PF2	PF0	PF1	PF2
0%	2.65	1.23	0.49	3.96	2.08	1.11	4.36	3.10	2.30
25%	2.80	1.04	0.33	4.56	2.04	1.19	4.61	2.71	2.14
50%	2.99	1.16	0.13	4.94	1.93	1.26	4.66	3.07	2.40

Note: Values in parentheses are percentage of the model without openings

4. CONCLUSIONS

Based on the experimental data of the pressure distributions on the face of the square building model without openings at various instants of time, a simplified bi-linear pressure profile is proposed for determining the maximum tsunami force acting on the structure, with the resulting force - wave height relation bounding the experimental results. The presence of openings allows water to enter the building, creating counteracting pressure on the inside of the upstream panel. Moreover, there exists a shielding effect which reduces the force acting on the rear panel. The tests show that there is a reduction in the wave force acting on the whole building in the order of 15% - 25% for the 25% opening configuration, and 30% - 40% for case of 50% opening. The corresponding reduction for the force on the front panel based on pressure recordings can be assumed to be 25% and 50%, respectively. The reduction in the tsunami force clearly demonstrates the benefit of openings in reducing the effect of tsunami on such buildings.

ACKNOWLEDGMENTS

The funding from the Department of Public Works and Town and Country Planning, Ministry of Interior and The Royal Golden Jubilee Project of the Thailand Research Fund is gratefully acknowledged. The support of Chulalongkorn University and the Asian Institute of Technology is highly appreciated. The authors greatly appreciate the valuable contributions of Prof. T. Takayama and Assoc. Prof. Pennung Wanitchai. The assistance of Dr. Somboon Siangchin and Mr. Surakai Banchuen is also acknowledged.

REFERENCES

Asakura, R., Iwase, K., Ikeya, T., Takao, M., Kaneto, T., Fuji, N., and Ohmori, M. (2002). The Tsunami Wave Force Acting on Land Structures. Proceedings of the 28th International Conference on Coastal Engineering , 1191-1202.

Cross, R.H. (1967). Tsunami surge forces. Journal of the Waterways and Harbors Division, Proceedings of the American Society of Civil Engineers 93:WW4, 201-231.

FEMA (2000). Coastal Construction Manual, FEMA 55 Report, Federal Emergency Management Agency, Washington, D.C.

Fukui, Y., Nakamura, M., Shiraishi, H., and Sasaki, Y. (1963). Hydraulic Study on Tsunami. Coastal Engineering in Japan, The Japan Society of Civil Engineers, Tokyo 6, 67-82.

Hamzah, M.A., Mase, H., and Takayama, T. (2000). Simulation and Experiment of Hydrodynamic Pressure on a Tsunami Barrier. Proceedings of the 27th International Conference on Coastal Engineering, 1501-1507.

Lukkunaprasit, P. and Ruangrassamee, A. (2008). Building Damage in Thailand in 2004 Indian Ocean Tsunami and Clues for Tsunami-Resistant Design. The Institution of Engineers Singapore Journal, Part A: Civil and Structural Engineering 1:1, 17 – 30.

Ramsden J. D. (1996). Tsunamis forces on a vertical wall caused by long waves, bores, and surge on a dry bed. Journal of Waterway, Port, Coastal, and Ocean Engineering 122:3, 134-141.

Ramsden J. D. and Raichlen F. (1990). Forces on vertical wall caused by incident bores. Journal of Waterway, Port, Coastal, and Ocean Engineering 116:5, 592-613.

Yeh, H. (2007). Design tsunami forces for onshore structures. Journal of Disaster Research 2:6, 531-536.

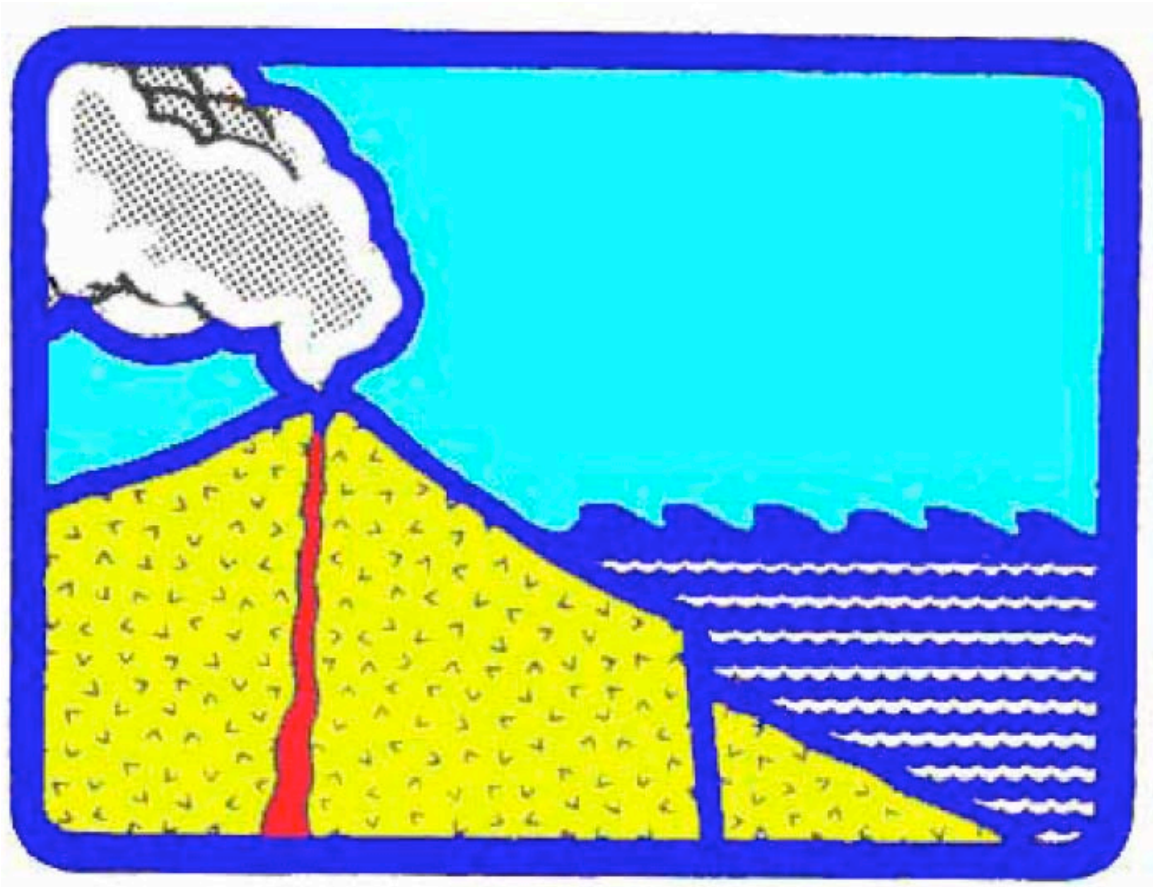

Tsunami Society International
1741 Ala Moana Blvd. #70
Honolulu, HI 96815, USA

WWW.TSUNAMISOCIETY.ORG